AN ABSTRACT OF THE THESIS OF

Nathan E. Schorn for the degree of Master of Science in Mechanical Engineering presented on June 6, 2019.

Title: Turbulent Combustion Analysis of Large Hydrocarbon Fuels in a Reduced Pressure Environment

Abstract approved: _____

David L. Blunck

The aviation industry is pushing for better fuels and gas turbine engines for several reasons: cost, emissions, and to a lesser extent high-altitude relights. One aspect that research has been focused on to help reduce costs, emissions and better understand high-altitude relights is studying the combustion behavior of the fuel being supplied (e.g., large hydrocarbon fuel). Understanding the combustion behavior of these fuels can bring new possibilities for incorporating alternative fuels and developing new combustor designs. Parameters that is commonly used to help measure and analyze the combustion behavior is the turbulent consumption speed and the mass burning flux. The objective of this work is to understand the effects of different flow conditions (e.g., varying Reynolds number and turbulence intensities), chemical sensitives (e.g., burning of different fuels at different equivalence ratios), and reduced pressure effects on the turbulent consumption speed and the mass burning flux.

The turbulent consumption speeds in this work ranged from 1 to 3 m/s for four different fuels: jet-A, ATJ Gevo, C10/TMB, and a surrogate fuel. The turbulent consumption speeds on average increased about 10% with a 30% decrease in pressure. ATJ Gevo was found to be the most sensitive to pressure effects out of the four fuels tested with increases of about 15 to 20% in turbulent consumption speeds. The turbulent burning flux values ranged from 0.5 to 2 kg/m^2-s. The burning flux on average decreased about 30% with a decrease in pressure. The turbulent consumption speeds where scaled by the zero-stretch laminar flame speed and the values ranged from 2 to 4. The sensitivity of the normalized turbulent consumption speed to pressure was

attributed to the changes in the density of the unburned mixture. At fuel-lean conditions, breaks in the flame tip were observed. A method was created to quantify when the flame became unstable. It was found that ATJ Gevo was the most sensitive to fuel-lean conditions, having the smallest stability range of the four fuels.

Turbulent Combustion Analysis of Large Hydrocarbon Fuels in a Reduced Pressure Environment

by

Nathan E. Schorn

A THESIS

submitted to

Oregon State University

in partial fulfillment of
the requirements for the
degree of

Master of Science

Presented June 6, 2019
Commencement June 2019

Master of Science thesis of Nathan E. Schorn presented on June 6, 2019.

APPROVED:

Major Professor, representing Mechanical Engineering

Head of the School of Mechanical, Industrial, and Manufacturing Engineering

---

Dean of the Graduate School

I understand that my thesis will become part of the permanent collection of Oregon State University libraries. My signature below authorizes release of my thesis to any reader upon request.

Nathan E. Schorn, Author

ACKNOWLEDGEMENTS

This research was funded by the U.S. Federal Aviation Administration Office of Environment and Energy through ASCENT, the FAA Center of Excellence for Alternative Jet Fuels and the Environment, project 13-C-AJFE-OSU-02 through FAA Award Number 13-C-AJFE-OSU under the supervision of Dr. Cecilia Shaw. Any opinions, findings, conclusions or recommendations expressed in this material are those of the authors and do not necessarily reflect the views of the FAA.

I would like to thank: Dr. Tim Lieuwen and colleagues (Georgia Tech) for burner specifications , Dr. Scott Stouffer (University of Dayton Research Institute) and the Air Force Research Laboratory (AFRL) for the vaporizer design, Dr. Tim Edwards (AFRL) for supplying the fuel, and Dr. Hai Wang's research group (USC) for laminar flame speed calculations and data.

I would like to thank everyone in the CIRE/Propulsion lab for their continued support and guidance. A special thanks to Jonathan Bonebrake for his continued support on the project. I would not have gotten as far as I did without him. I would also like to thank Aaron J. Fillo for building the ground work for this project and his continued guidance. I would also like to thank the army of undergrads that have worked with me on the project throughout the 3 years that I was on it: Mila Bakker, Delphine Le Bron Colon, Brandon Pendergrass, Ankit Agarwal, Ammar Alkhalifa, and Zohar Hoter.

I would like to thank Dr. David Blunck for the opportunity of working on this project and his continued guidance and support through the 3 years I worked for him. A special thanks to Dr. Nancy Squires who originally spurred me on to continue my education and Dr. Javier Calvo-Amodio for his recommendation into graduate school.

Finally, I would like to thank my family and friends who helped me along this roller coaster of a ride that we call graduate school.

TABLE OF CONTENTS

LIST OF FIGURES

LIST OF FIGURES (Continued)

LIST OF TABLES

LIST OF APPENDICES

LIST OF APPENDIX FIGURES

LIST OF APPENDIX TABLES

Chapter 1: Introduction

1.1 Motivation

The aviation industry is pushing for better fuels and gas turbine engines for several reasons: cost, emissions, and to a lesser extent high-altitude relights. First, the average cost for fuel and oil of a typical jetliner over its life span can be upwards of 34.6 billion dollars [1]. This accounts for 27% of the total cost for the jetliner. Developing more efficient fuel or jet turbines can help drastically reduce this cost. Second, the transportation sector is responsible for 27% of the total greenhouse gas emissions in the world [2]. There have been great strides in reducing emissions in the ground transportation with increases in electrical or bio-diesel engines but, for the aviation industry, alternative fuels are still far from being practical [3]. This is because jet aviation fuel has a greater fuel energy density (energy per unit mass) than their alternative fuel counter parts [4]. This is a major factor in aviation because weight is a critical issue, so it is advantageous to create as much energy as possible with as little weight as possible. Developing an understanding of combustion behavior of the fuel being supplied to the engines can help incorporate alternative fuels within the industry. Finally, high-altitude relights happen infrequently, but can lead to serious consequences if not handled properly. It is mandatory by the Federal Aviation Administration and European Aviation Safety Administration that engines meet certain requirements for high-altitude relight scenarios [5], [6]. Designing cutting edge turbine engines or afterburners will necessitate understanding of low pressure combustion to help prevent these events and meet safety standards.

An effort has been put forth to understand the fundamental combustion behavior of jet aviation fuel at engine-like conditions (i.e., at relevant engine pressures and temperatures) for the development of alternative fuels and new gas turbine engines [7]–[14]. There have been great strides in understanding large hydrocarbon fuels in the laminar environment, but little research has been done in a turbulent environment [8], [11], [15]. This is problematic because the combustion process in a jet engine combustor is highly turbulent [11], [16]. Turbulent flame speed is one metric used in the evaluation of turbulent combustion behavior for small hydrocarbons [16]–[20]. Evaluating the turbulent flame speed is advantageous because it is dependent on the

chemical kinetics of the combustion process and unsteady vortices that form within [16], [17]. Further research has expanded the analysis of turbulent flame speed with respect to increased pressures, but little research as been done on the effects of reduced pressures [18]–[21]. Furthermore, the effect of the burning behavior of large hydrocarbon fuel on the turbulent flame speed is still not relatively understood [13], [20]. Using the turbulent flame speed can help compare different chemical effects created by burning of different large hydrocarbon fuels and sensitivities to a reduced pressure environment.

Operating turbine engines on minimal amounts of fuel (fuel-lean) can help produce less emissions and is more cost effective [10]. However, operating at lean conditions can cause combustion stability issues leading to blow-off, or failure to ignite [7]. Stability of the combustion is highly dependent on burner geometry and operating conditions, but having an understanding of the fuel being supplied can greatly influence combustor design [22]. To further reduce the cost and emissions associated with burning large hydrocarbon fuels, understanding the stability of the combustion can help in the development of different fuels that can combust at even lower fuel-lean operating conditions.

Aviation fuels are made up of hundreds of different chemical constituents (mainly large hydrocarbons) to achieve various desired results (e.g., lower extinction temperatures, resistance to freezing, etc.). This can be problematic when trying to model or test jet aviation fuels because of the complexity of their composition. This makes surrogate (jet-like) fuels appealing for modeling and testing because of their relatively simple composition [8], [9], [14]. Simple surrogate fuels are typically only made with three large hydrocarbon chains and consist of at least an aromatic, n-alkane, and an iso or cyclo-alkane [23]. Having an understanding of how a surrogate fuel behaves in a combustion environment and comparison to its more complex counterparts is needed to asset the usefulness of these fuels.

1.2 Objectives

The goal of this study is to ascertain the combustion behavior of large hydrocarbon fuels. The large hydrocarbon fuels are subjugated to a turbulent burning environment, reduced pressures, and combustion instabilities to compare the differences in their combustion behavior. The specific objectives of this study to achieve these goals include the following:

1. Identify how reducing pressure affects the turbulent consumption speed of jet and jet-like

fuels.

2. Ascertain how fuel chemistry alters the pressure sensitivity of turbulent combustion by the use of various jet-like fuels.

3. Ascertain how fuel chemistry alters the stability of turbulent combustion at atmospheric and sub-atmospheric pressures.

4. Identify potential discrepancies in the turbulent burning behavior of surrogate and practical jet fuels.

1.3 Outline

Chapter 2 is a manuscript intended for submission for a peer-review publication. In this chapter, the effects of pressure on turbulent combustion behavior of large hydrocarbon fuels are evaluated. The evaluation of the combustion behavior was done by analyzing the turbulent consumption speed, the turbulent burning flux, and the instabilities of fuel-lean combustion. The results from the analysis are dimensionally scaled to discern turbulence effects on the combustion behavior in a reduced pressure environment.

Chapter 3 is a manuscript intended for submissions as a brief communication. In this chapter the burning behavior of a 3-component surrogate fuel is compared to a jet fuel commonly used in industry (jet-A). The turbulent consumption speed, turbulent burning flux, and the combustion stability are evaluated for the comparison of these two fuels. The results of this comparison show the differing chemical kinetic sensitives to a turbulent combustion environment.

Finally, Chapter 4 summarizes the results from the previous chapters and the conclusions made. This chapter also suggests future studies..

Chapter 2: Pressure Effects on the Turbulent Consumption Speed and Flame Stability in Large Hydrocarbons Fuels

Chapter 2 is work being submitted for peer-review publication on the effects of reduced pressure on a turbulent Bunsen jet fuel flame. The work covers the combustion behavior of the Bunsen flame in a low pressure environment of various jet and jet-like fuels using parameter scaling techniques. Further presented in this work is a stability analysis on various jet and jet-like fuels at different pressure conditions. The primary author of this article is the author of this thesis. The primary author provided most of the experimental setup, data collection, data analysis, and resulting conclusions from the data collected. Various co-authors provided help in experimental setup, data collection, and conclusions. The expected co-authors are as follows: Jonathan M. Bonebrake, Zohar Hoter, Aaron J. Fillo, and David L. Blunck.

2.1 Introduction

Gas turbine engines used for propulsion generally operate at elevated pressures; however, high altitude relight and afterburner scenarios can require operation at sub-atmospheric pressures [24]. Reignition and eventual stable combustion at reduced pressures can be challenging to analyze since these systems operate in conditions that are highly turbulent [14]. Numerous efforts have been made to understand turbulent combustion processes within these systems, including fuel effects on engine performance [7], [8], [10], [11], [14], [23]. Turbulent flame speed is one metric that is used in the evaluation of the combustion behavior of fuels [18]–[20]. Unfortunately, the combustion community's understanding of the combustion behavior of jet fuels over a range of pressures, including sub-atmospheric conditions, is limited at best [20].

Flame stability is an essential aspect of operating gas turbine engines, both in a main combustor and in afterburners. The stability of gas turbine engines depends on the fuel being burned as well as the burner geometry [22]. Having a better understanding of the stability of flames burning aviation relevant fuels, even for canonical burners, can be used to provide insights into potential sensitivities of combustor stability when those fuels are burned.

2.2 Background

2.2.1 Pressure Effects

Pressure Effects in Laminar Flames

Studies of laminar flame speeds sensitivities to changes in pressure are of interest because turbulent flame speeds are controlled by the laminar flame speed of the mixture. In short, the laminar flame speeds of fuels are inversely proportional to the pressure [8], [16], [25]–[28]. For example, Egolfopoulos et al. [26] studied the pressure effects on the laminar flame speed of CH_4 flames and found that as pressure increased the laminar flame speed decreased. The sensitivity of the laminar flame speed (S_u^o) to pressure is attributed to several processes. First, laminar flame speeds are inversely proportional to the unburned density (ρ_u) of the reactants, so as the density of the reactant increases or decreases the laminar flame speed will decrease or increase (respectively). The laminar burning flux (f^o), which is defined as $f^o = \rho_u S_u^o$, has been used to discern the effects of changes in pressure on fuel consumption rates with respect to density. As pressure increased, the burning flux increases for CH_4 and hydrogen flames [16], [26]. This observation shows that mass consumption rates increased with pressure, as expected because of greater concentrations of reactants, but decrease the associated laminar flame speed. A second cause of laminar flame speeds decreasing with increasing pressure, is the effect of increased pressure on three-body termination reactions. To determine this effect the overall reaction order (n) is calculated from the laminar burning flux and the pressure (P), $n = 2\frac{\partial \ln f^o}{\partial \ln P}$. Based on reaction order analysis three-body reactions become more important as pressure increased, ultimately reducing overall reaction rates slowing down the laminar flame speed [8], [16]. The opposite is true for decreasing pressure; two-body reactions become more important, which accelerates reaction rates.

Most studies on the effect of pressure on laminar flame speeds have been focused on small hydrocarbons fuels [16], [20], [25]–[27], [29], but several studies have evaluated the sensitivities of large hydrocarbon fuels (i.e., liquid at room temperature). Hui and Sung [8] utilized a twin flame burner to measure the laminar flame speeds of ten transportation relevant fuels including jet-A, S-8, and a four-component jet-A surrogate. All fuels showed a similar sensitivity to pressure; laminar flame speeds decreased as pressure increased. This study also showed that the laminar burning flux increased with increasing pressure, showing the importance of considering

density changes when determining fuel consumption rates. The overall reaction order was then determined from the laminar burning flux to help evaluate the importance of the termination reaction mechanisms within the combustion process. It was found that three-body termination reactions reduced the reaction rates and slowed the flame speeds as pressure increased, similar to the work performed by Egolfopoulos et al. [26]. These are important findings because they show that even large hydrocarbon fuels, with their more complex reaction kinetics, have pressure sensitivities similar to their gaseous counterparts.

Pressure Effects in Turbulent Flames

Considerable research has been performed to understand the effect of pressure on the turbulent flame speeds of hydrocarbon fuels, in particular for gaseous fuels [18]–[21], [30]. Kobayshi et al. [31] studied the effects of pressure (e.g., up to 1 MPa) and turbulence intensity on turbulent flame speeds of CH_4/air and C_3H_8/air flames. As pressure increased there was relatively little effect on the turbulent flame speed of these fuels. However, normalized turbulent flame speed (by laminar flame speeds, S_T/S_L) increased with increasing pressure. A subsequent study by Kobayashi et al. [19] attributed the increase in the normalized turbulent flame speed with pressure to an increase in the wrinkling of the flame front (thus increasing the area) and a decrease in the S_L. The increase in normalized turbulent flame speeds reported by Kobayashi has been verified by the work of others [18], [20], [21], [32]. However, these works found that the turbulent flame speed increases as pressure increases. For example, Venkateswaran et al. and Marshall et al. [18], [30], [33] performed several studies on H_2/CO Bunsen flames studying pressure effects on the stretch rates of the Bunsen flame. The research found that pressure influences the turbulent flame speed by altering the chemical time scales on the Taylor-micro scale, which effects the stretch rate at the leading point of the flame. Another study by Fragner et al. [21] attributed the increase in wrinkling to the stretching of the turbulent energy spectrum towards smaller turbulent scales by an increasing wave number with pressure. Both studies found that the pressure affects the smaller times scales in both the chemical kinetics and in the fluid flow, thus increasing the turbulent flame speed. Of note, these studies have focused on small hydrocarbon fuels and very little research has been done on large hydrocarbons.

2.2.2 Stability

Classifying stability and extinction limits of the combustion process can vary depending on burner geometry type. One extinction phenomenon that has been considered is tip quenching of a Bunsen flame [12], [34]–[37]. Tip quenching is when the tip of the Bunsen flame experiences a local extinction event and a break in the flame front occurs [34], [37], [38]. The tip of the Bunsen flame experiences the most negative stretch, thus making is the most susceptible to breaking. Breakage is attributed to the balance between mass and heat diffusive effects and is dominated by the turbulent eddies, causing the tip of the flame to extinguish [34]–[36]. Carbone et al. [12] studied the phenomenon of tip quenching in turbulent Bunsen flames for C1 through C8 hydrocarbons. By using a high speed camera and an image intensifier, they where able to capture the large vortical structures that form within the flame. They found that as the height of the flame increases the integral length scale of the combustion eddies increases to a maximum point, than sharply drops off to zero. This drop-off was classified to be the location at which the flame tip opens. They discovered that for high Reynolds number flows, wrinkling in the flame front was more pronounced than for lower Reynolds number flows, which could be attributed to either quenching or burnout of smaller coherent reactivity structures as they are convected further downstream in the jet. Similar to Carbone, Wang et al. [37] investigated Bunsen tip quenching but with hydrogen flames. By using an OH-PLIF system, they were able to analyze the local Karlovitz number for various flame conditions. They discovered that the Bunsen flame tip will extinguish when the local Karlovitz number approaches a constant value, irrespective of hydrogen fraction and outlet velocity. This observation shows that the Bunsen flame tip starts to experience local extinction when the tangential flow time is comparable to normal chemical reaction time, which is similar to the results reported for counterflow flames with positive stretch [9].

It has been shown that turbulent eddies dominate the process, but are still coupled by thermo-diffusive effects [12], [20], [37]. An understanding of thermal effect could lead to more insight on the stability of flames. Kumar et al. [9] examined extinction limits for large hydrocarbon fuels (i.e., jet fuels), using a twin stagnation flame configuration. They discovered that, with lean flames, extinction occurs with finite separation distance, while rich flames exhibit a merging of two luminous flamelets. It was suggested that the reactivity of a positively stretch flame with a Lewis number smaller than unity increase with increasing stretch rate [9], [16], [34]. Kumar's result showed that with a sub-unity Lewis number (Le $<$ 1), rich jet fuel mixtures extinguish

in merged flame mode because of the incomplete reactions. While for a Le $>$ 1, lean jet fuel mixtures extinguish because of the non-equidiffusion effects. Later studies done by Kumar et al. [9] analysed more complex hydrocarbon chains (i.e., jet fuels) on the same burner configuration. They found that the extinction rates were lower near lean conditions than their single component counterparts and, at rich conditions there was little difference at all.

2.2.3 Objective

With this background and motivation, the objective of this study is to ascertain the effects of changes in pressure on the turbulent flame speed and stability of flames burning large hydrocarbon fuels. Specifically, measurements are collected at pressures of 1 and 0.7 atmospheres (101 kPa and 71 kPa respectively). A range of fluid mechanic conditions (e.g., various Reynolds numbers, turbulent intensities, and pressures) are considered. A jet and two jet-like fuels are included in the study to allow the chemistry effects on pressure sensitivity and stability to be better understood.

2.3 Methodology

2.3.1 Experimental Setup

The experimental arrangement for conducting the turbulent consumption speed measurements is illustrated in Figure 3.1 and includes a fuel vaporizer, Bunsen burner, and pressure chamber. The Bunsen burner configuration was based on the design developed by Venkateswaran et al. [33]. A thermal mass flow meter and a syringe pump were used to meter the air and fuel, respectively. The fuel was injected through a siphon air-atomizing nozzle into the vaporizer, where it mixed with the incoming air. The fuel/air mixture was heated to temperatures near 475 K within the vaporizer. The mixture flowed through a turbulence generator inside the Bunsen burner. The turbulence generator allowed for control over the ratio of the turbulent fluctuating velocity (u_{rms}) and the bulk flow velocity (U). The turbulence generator produced estimated ratios, or turbulence intensities (u'_{rms}/U), of approximately 10 to 20% at the burner exit [13]. A premixed methane/air pilot flame ignited the mixture and anchored the Bunsen flame to the burner. The Bunsen and pilot flames were contained within an optically accessible pressure chamber. The experimental arrangement allowed for control over the Reynolds number of the

flow, the equivalence ratio or the ratio of fuel-to-air in the mixture (ϕ), the turbulence intensity (TI), and the pressure. Fuel flow rates, Reynolds numbers, and fuel-to-air ratios where calculated using fluid properties provided by EES, see appendix D.

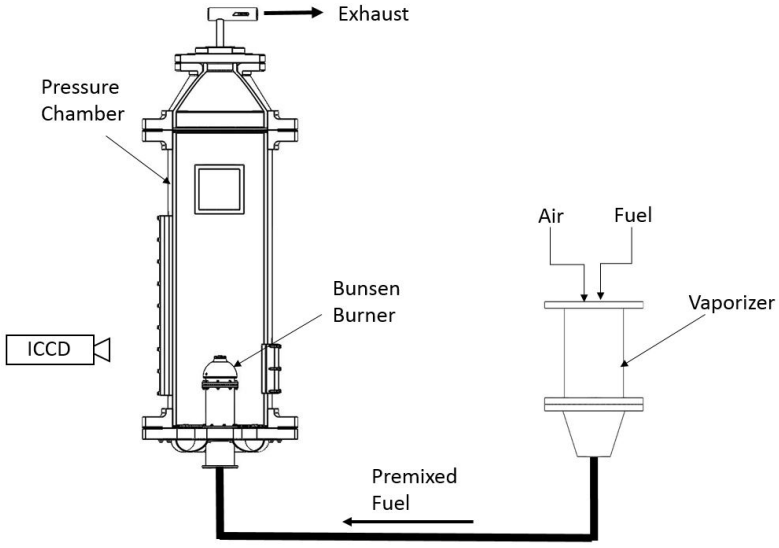

Figure 2.1: Schematic of the turbulent Bunsen burner and vaporizer.

The fuel types examined were jet-A (a conventional jet fuel) and two test fuels (ATJ Gevo and and C10/TMB) that have similar thermophysical properties to jet-A, but different chemical compositions and molecular weights (see table 2.1). The similarities in the lower heating value is important because the flame speed is often sensitive to temperature [8], [16], [18], [19]. Similar lower heating values will provide similar flame temperature helping control the sensitivity to temperature. Each fuel was tested at a Reynolds numbers of 5,000 and 10,000, turbulence intensities of $\sim$10% and $\sim$ 20%, and pressures of 101 kPa and 71 kPa (atmospheric and sub-atmospheric respectively). Table 2.2 shows the compositions of three chemical compounds that previous research has shown to be important when evaluating turbulent consumption speed and stability sensitivity [39]. The naming convention for the fuel is as follows; "Category A", which represent properties seen in current industry jet-fuel and "Category C" which are test fuels [23]. Note that the constituents within A2 do not add up to 100%, because of other components within the fuel (e.g., cyclo-alkanes).

Table 2.1: Thermophysical properties of the three fuels tested [23].

Fuel	Average Molecular Formula	Lower Heating Value (MJ/kg)	Molecular Weight (g/mol)	Density (kg/m^3)
jet-A (A2)	$C_{11.4}H_{21.8}$	43.06	159	0.803
ATJ Gevo (C1)	$C_{12.6}H_{27.2}$	43.88	178	0.760
C10/TMB (C5)	$C_{9.7}H_{18.7}$	42.90	135	0.769

Table 2.2: Breakdown of three chemical compound chains within the three fuels tested [23].

Fuel Designation	Aromatics (% vol)	iso-Alkanes (% vol)	n-Alkanes (% vol)
jet-A (A2)	11.2	39.1	27.2
ATJ Gevo (C1)	0	near 100	0
C10/TMB (C5)	27.3	54.2	18.5

2.3.2 Data Analysis

Turbulent Consumption Speed

An Andor Solis ICCD camera was used to measure chemiluminescence emissions from the turbulent Bunsen flame, refer to figure 3.1. The camera is sensitive to wavelengths between 200 and 1100 nm and is capable of capturing emissions from OH* and CH* chemiluminescence [40]. OH* and CH* chemiluminescence have been shown to be markers of the flame front used in the calculation of the turbulent consumption speed [33]. The camera sampled images at a rate of 2 Hz for a total of 360 images. These images were averaged to obtain the average flame brush area displayed in Figure 2.2a. This area was used in the definition of the turbulent consumption speed [17],

$$S_T = \frac{\dot{m}}{A_{\langle c \rangle}\rho_u}, \tag{2.1}$$

where $\dot{m}$ is the mass flow rate, $A_{\langle c \rangle}$ is the time averaged area of flame brush, and ρ_u is the unburned density. The parameter $\langle c \rangle$ is the progress variable, which is a measure of reactant

consumption through the flame brush [31]. Where $\langle c \rangle$ = 1 corresponds to the burned surface area of the flame front and $\langle c \rangle$ = 0 corresponds to the unburned surface area. Kobayashi [31] found that a value of $\langle c \rangle = 0.5$ gives a good representation of the mean inner surface of the flame brush (i.e., the location of the maximum intensity of the flame brush), which can be used to determine the turbulent consumption speeds, and is therefore used in the area calculation. To determine the mean area of the flames from the averaged image, an approach similar to that used by Fillo et al. [39] was used, as illustrated in Figure 2.2. The averaged image background was subtracted to eliminate emissions from the pilot flame, cropped of unnecessary information, corrected for asymmetry, filtered for noise by a median filter, and processed through a three point inverse Abel convolution scheme [41]. The Abel transform returns a calculated three-dimensional image from the averaged two-dimensional flame image. The centerline, outlined in red in Figure 2.2a, is taken from the resulting data and plotted against the axial distance. The $\langle c \rangle = 0.5$ contour corresponding to the flame front location is determined by fitting a Gaussian curve to the resulting intensity profile. The axial location of the apparent flame height is found by the peak intensity of the Gaussian curve (corresponding to the $\langle c \rangle = 0.5$ contour). With the height known, the flame area (treated as a cone) was determined using the radius of the burner as the base of the cone.

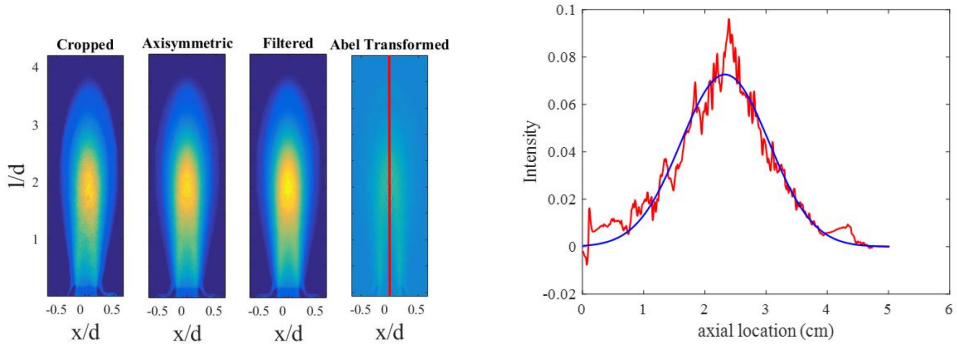

Figure 2.2: Figure 2.2a shows the time averaged flame image as it is being processed and is graphed against the axial location (l) and the radial distance (x) normalized by the diameter of the jet (d). From left to right, the image is cropped, corrected for asymmetry, filtered, and transformed by the Abel deconvolution. Figure 2.2b is the centerline intensity profile of the Abel deconvolution, a Gaussian curve (blue) is fitted to the centerline intensity (red).

Stability

To quantify the instabilities of the flame front, a qualitative approach is used to first observe the tip quenching phenomenon. Figure 2.3 shows the visual images of the Bunsen flame at conditions considered to be stable and unstable.

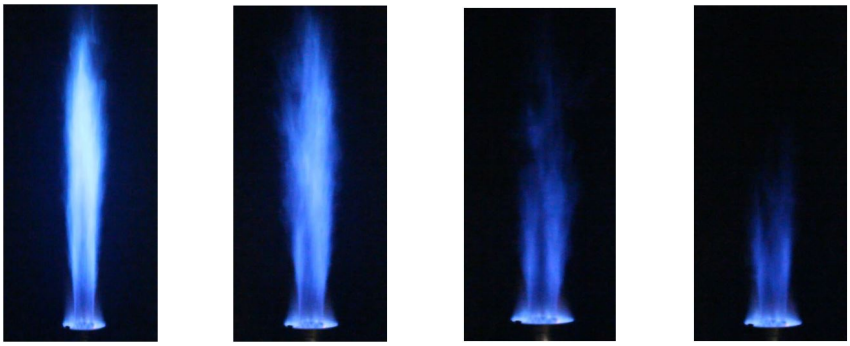

(a) ϕ value of 0.9. **(b)** ϕ value of 0.8. **(c)** ϕ value of 0.7. **(d)** ϕ value of 0.6.

Figure 2.3: Visual inspection of full flame tip ignition (panel a), quasi ignition/quenching (panels b and c), and full tip quench (panel d).

Figure 2.3a represents full tip ignition, Figure 2.3b and 2.3c are quasi ignition/quenching, and the tip is fully quenched in Figure 2.3d. The quasi ignition/quenching is of interest because it is at this point that fuel starts to break through the flame front. These conditions are highly transient, so a Phantom veo 710 high speed camera is used to image the flame. Three sets of 16,000 images were used to create an averaged flame image. Each set was taken at 8,000 frames per second. The radial distribution of the averaged flame image was plotted at the height of the maximum intensity of each flame image, see Figure 2.4. The flame is classified as unstable when either a biomodal distribution forms or a sharp decrease in intensity towards the middle of the flame (r = 0) is observed, followed by a gradual decrease. These distributions form because the maximum intensity is no longer at the center of the flame, but shifts to the edges of the flame.

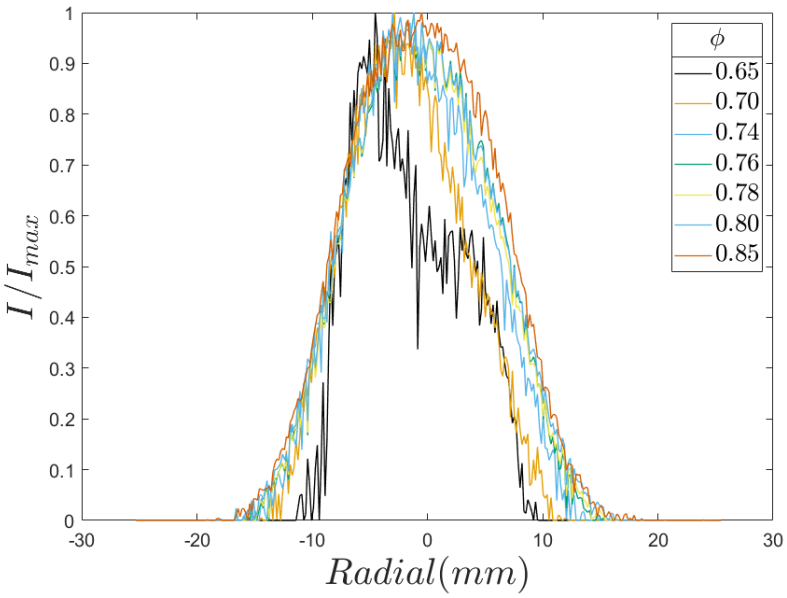

Figure 2.4: Radial profile example of tip quenching. Depicted here is jet-A at a Reynolds number of 10,000 and a TI of 20%. From the figure it is recognized that the flame becomes unstable between $0.65 < \phi < 0.70$.

2.4 Results/Discussions

2.4.1 Turbulent Consumption Speed

Turbulent consumption speeds are reported for flames with a Re of 5,000 and 10,000, 10% and 20% turbulent intensities (TI), and at pressures of 101 kPa and 71 kPa in Figure 2.5.

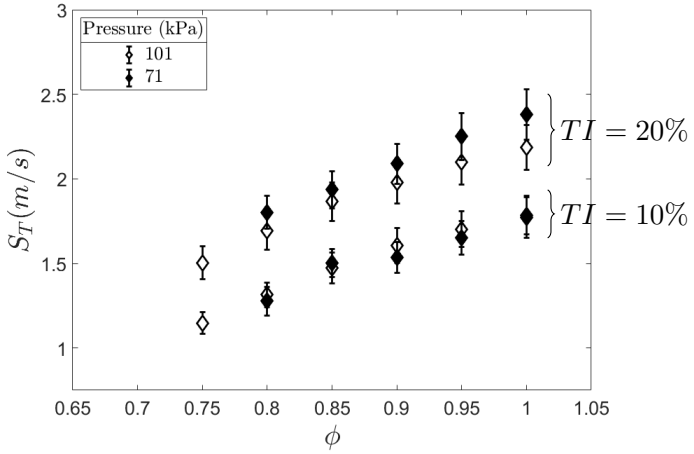

(a) Re of 5,000.

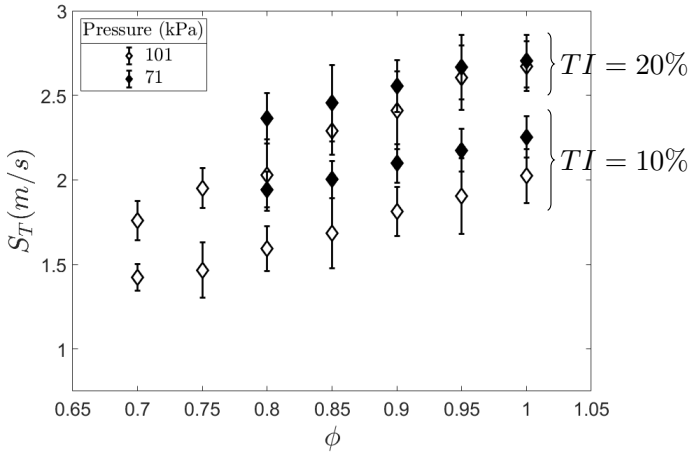

(b) Re of 10,000.

Figure 2.5: Turbulent consumption speed values for jet-A at different equivalence ratios. C1 and C5 both exhibit similar behavior and have been omitted for clarity.

Figure 2.5 shows only turbulent consumption speeds for A2, C1 and C5 where omitted for clarity. Atmospheric (101 kPa) and sub-atmospheric (71 kPa) are open and closed symbols respectively. Labeled on Figure 2.5 are the two turbulence intensities cases (10 and 20%) that each have atmospheric and sub-atmospheric values. For a Re of 5,000 (top panel) and a TI of 20%, the turbulent consumption speeds typically increased with a decrease in pressure. In contrast, for the low turbulence intensity condition (e.g., 10%), as pressure decreases there are negligible changes in the turbulent consumption speed. This pressure sensitivity is attributed to the increase in the turbulent fluctuations between high and low intensity conditions, as discussed later. In contrast, for a Re of 10,000, as the turbulence intensity is decreased from 20% to 10%, it is the low intensity conditions that experience the greater pressure sensitivity. It is noted that the pressure sensitivities just described are opposite to those reported previously for small hydrocarbon fuels [18], [20], [21]. It is observed that for the flames with Re of 10,000, a greater sensitivity of flame speeds to pressures occurs at lower ϕ values ($0.80 < \phi < 0.85$), while at higher ϕ values the turbulent consumption speeds are statistically similar. The greater difference at lower ϕ values is attributed to potential breaks in the flame front, as discussed later. Openings in the flame front allow fuel to break through and not be consumed, tending to bias flame speeds higher.

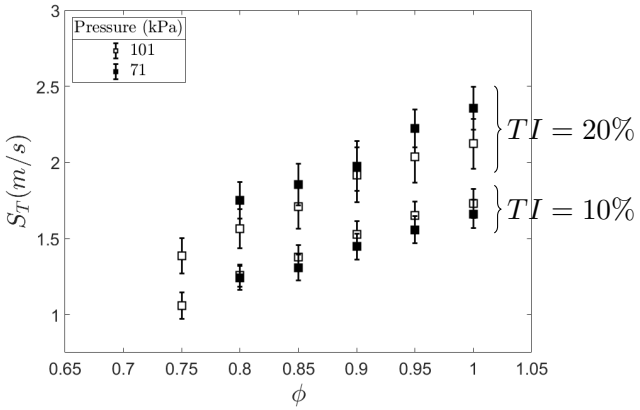

(a) C1 turbulent consumption speeds at a Re of 10,000.

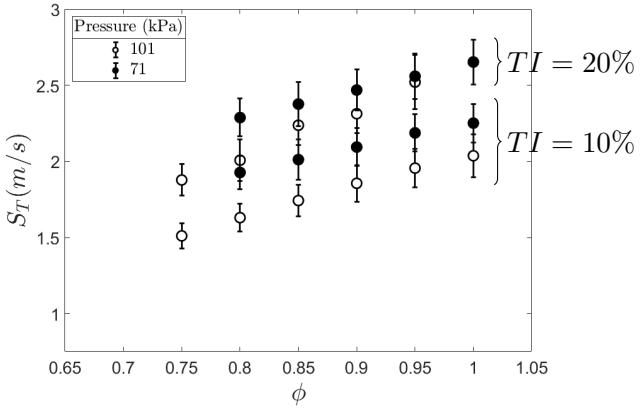

(b) C5 turbulent consumption speeds at a Re of 10,000.

Figure 2.6: Turbulent consumption speed values for C1 and C5 at a Re of 10,000.

Figure 2.6 reports the turbulent consumption speed for C1 and C5 at a Re of 10,000. Reynolds number of 5,000 for the two test fuels showed similar trends to that of A2 and are presented in appendix A. For C1 (top panel), at turbulent intensity of 10%, a statistically different increase in turbulent consumption speeds is seen with a decrease in pressure. However, for a turbulent intensity of 20%, no clear difference is seen until a ϕ value of 0.85. For C5 (bottom panel), at a turbulent intensity of 10%, the turbulent consumption speeds are statically similar except for ϕ values of 0.8 and 0.85. At a turbulent intensity of 20%, the turbulent consumption speeds at atmospheric and sub-atmospheric pressures are statically similar. A2 and C5 have similar differ-

ences, with absolute differences ranging from 0 to 0.3 m/s, but have discrepancies near lower ϕ values. C1 shows the greatest sensitivity to pressure changes, especially for the 10% turbulence intensity case, with difference ranging from 0.25 to 0.35 m/s. It is possible the differences seen is caused by the opening of the flame tip near lower ϕ values, biasing the consumption speed higher, which will be discussed later in this section.

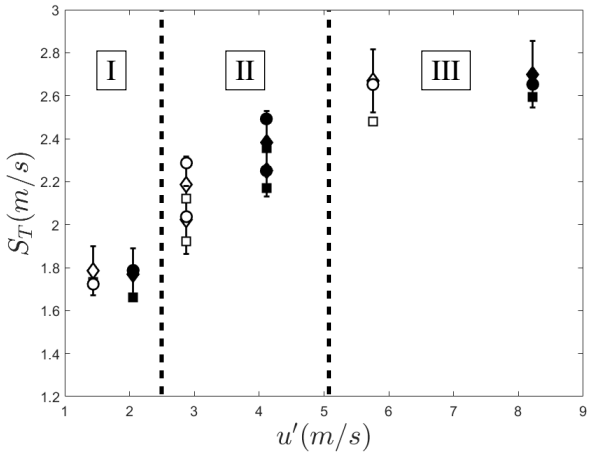

(a) ϕ = 1.

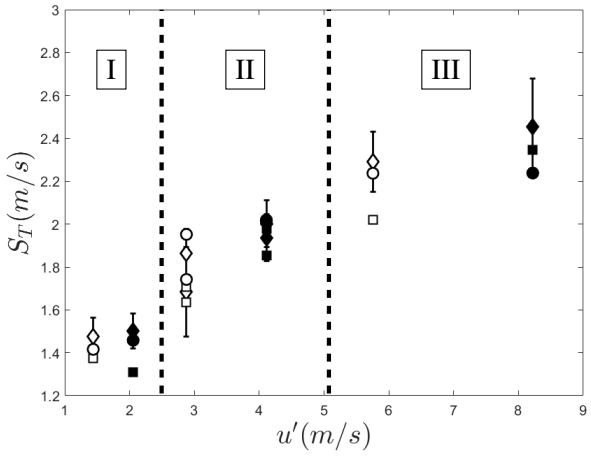

(b) ϕ = 0.85.

Figure 2.7: Turbulent consumption speed values at various turbulent fluctuating velocities. Atmospheric (101 kPa) and sub-atmospheric (71 kPa) are open and closed symbols respectively. Representative error bars are shown for A2 but omitted for C1 and C5 for clarity.

Figure 2.7 shows the turbulent consumption speeds relative to the velocity fluctuations for flames with ϕ value equal to 1 (top panel) and 0.85 (bottom panel). Atmospheric (101 kPa) and sub-atmospheric (71 kPa) are open and closed symbols respectively. Artificial regions I through III where created to better represent the trends discussed. These results are useful for better understanding the effect of turbulent fluctuations on the turbulent consumption speed. It is observed for both ϕ values, as turbulent fluctuations increase there is an increase in turbulent consumption speed, consistent with what has been reported previously [16], [19], [20]. It is noted that sub-atmospheric pressure flames (filled symbols) experience larger velocity fluctuations at a given Re than flames at atmospheric conditions. As pressure is decreased the bulk velocity is increased (to fix the Re) and as a results the velocity fluctuations increase as well. It is interesting to note at $\phi = 1$ for low and high turbulent fluctuations (regions I and III), there is relatively little change in turbulent consumption speed with a decrease in pressure for all three fuels. Region II for $\phi = 1$, however, shows an increase in turbulent consumption speed between the two pressure cases. For $\phi = 0.85$ the same trends are observed in Regions I and II, but for region III an increase in turbulent consumption speed is seen with a decrease in pressure. The different sensitivities to pressure, depending upon the magnitude of the velocity fluctuations, is attributed to the increase in the turbulent fluctuations.

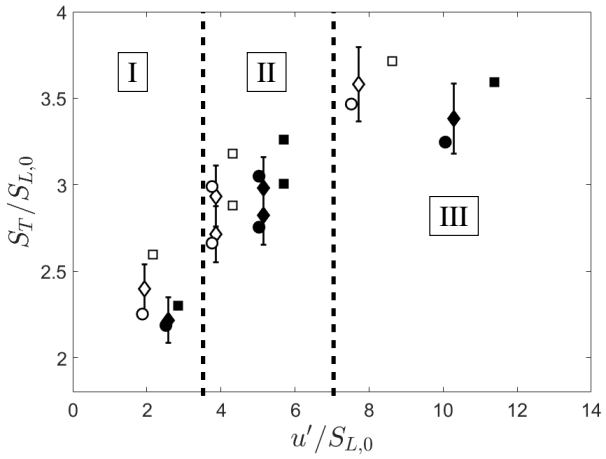

(a) ϕ = 1.

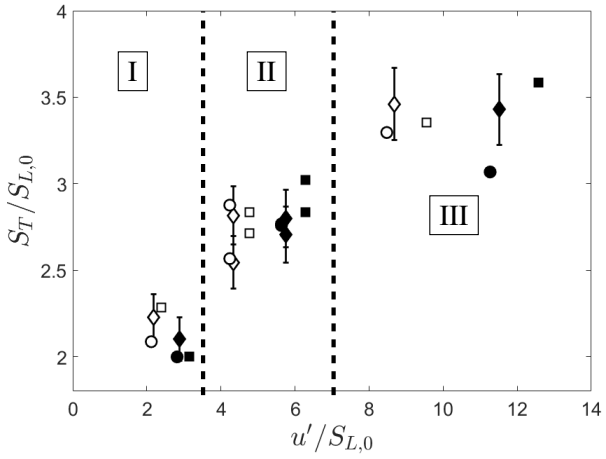

(b) ϕ = 0.85.

Figure 2.8: Normalized turbulent consumption speed compared to the normalized turbulent fluctuations by the zero-stretch laminar flame speed. Representative error bars are shown for A2 but omitted for C1 and C5 for clarity.

Figure 2.8 shows the turbulent consumption speeds and turbulent fluctuations normalized by the zero-stretch laminar flame speed ($S_{L,0}$). The zero-stretch laminar flame speeds were calculated using HyChem [42]. The HyChem approach, or hybrid chemistry, decouples fuel pyrolysis from the oxidation of fuel pyrolysis products. This is advantageous because high-temperature combustion of large hydrocarbon fuels effectively occurs in two separate stages:

fuel pyrolysis first and then the oxidation of the pyrolysis products. The HyChem model has been proven for laminar flame speeds at a pressure of 101 kPa. The model has yet to be proven for 71 kPa, but the trend in the laminar flame speed for the three large hydrocarbon fuel behave similarly to what is seen in literature [8], [26], [27]. The uncertainty in the laminar flame speeds has been taken into account within the representative error bars. For Figure 2.8, in regions I and III, it is seen that as pressure decreases, $S_T/S_{L,0}$ decreases as well. This is similar to what is seen in literature where $S_T/S_{L,0}$ increases with increasing pressure for small hydrocarbon fuels [18]–[21], [32]. Again however, in region II, an increase is seen with a decrease in pressure.

Figure 2.9 shows $u'/S_{L,0}$ for all ϕ values for better insights into the effects of pressure on the normalized turbulent consumption speed values. As $u'/S_{L,0}$ increases, a greater disagreement is observed between atmospheric and sub-atmospheric (open and closed symbols respectively) as $S_T/S_{L,0}$ increases. It is observed that when comparing regions I to III, the difference between the two pressure cases decreases as it approaches higher $u'/S_{L,0}$ values. This shows that $S_T/S_{L,0}$ becomes less sensitive to pressure with increasing $u'/S_{L,0}$.

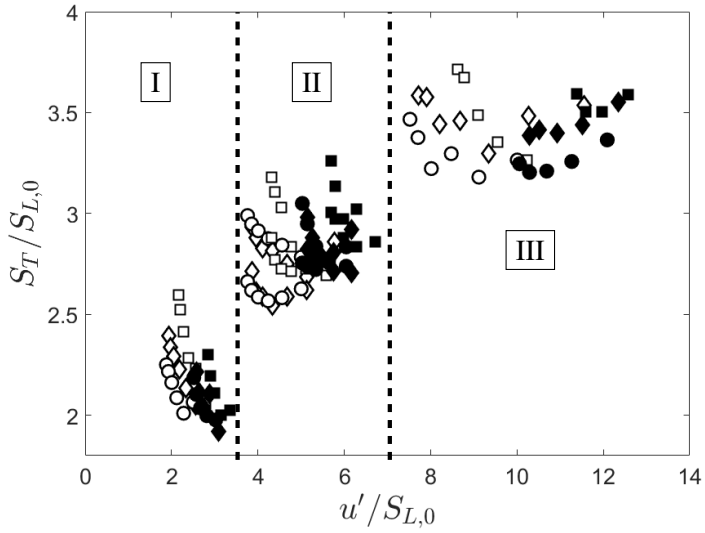

Figure 2.9: Normalized turbulent consumption speed compared to the normalized turbulent fluctuations by the zero-stretch laminar flame speed. Error bars have been omitted for clarity, but are on the order of +/- 6%.

The fluctuating velocities where further normalized by the ratio of the ambient pressure (P)

to atmospheric pressure (P_0) to allow comparison to other studies considering pressure effects on the turbulent flame speed. Shown in Figure 2.10 are two pressure correlations developed from Kobayshi's experimental data from CH_4/C_2H_4 and C_3H_8 flames [19]. The large hydrocarbon fuels from this study behave similarly with the C_3H_8 correlation, but do not follow CH_4/C_2H_4 correlation. The results shows a decrease in magnitude of $S_T/S_{L,0}$ as the size of the hydrocarbon increases. The correlations sharp increase in $S_T/S_{L,0}$ with low $(P/P_0)(u'/S_{L,0})$ is attributed to a greater influence of Darrieus-Landau hydrodynamic instabilities of the flame front caused by the changes in density. Based on the similarity between Kobayshi's correlations and the large hydrocarbon fuels reported here, it is proposed that the large hydrocarbon fuels are being affected by the same hydrodynamic instabilities caused by the density change.

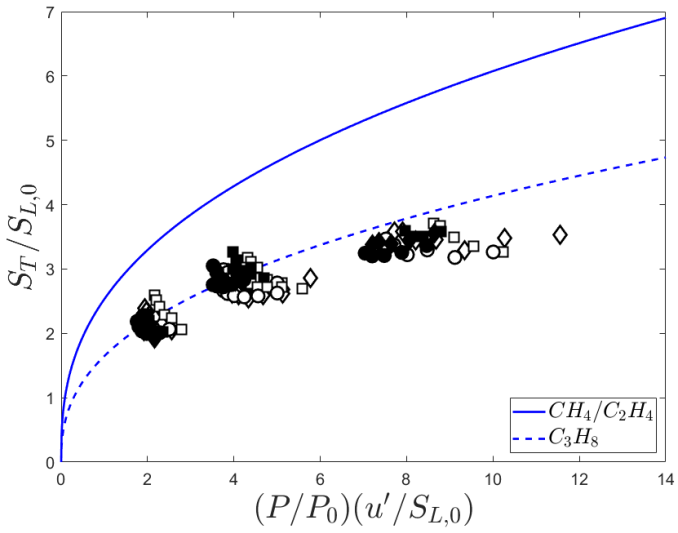

Figure 2.10: $u'/S_{L,0}$ normalized by the pressure ratio. Blue lines represent correlation developed by Kobayashi [19].

2.4.2 Mass Burning Flux

The sensitivity to changes in the mass consumption rate of fuels with changes in pressure can be readily discerned by considering the mass burning flux. Adapting the laminar burning flux definition, the relationship for the turbulent burning flux ($\dot{m}''_T$) is derived,

$$\dot{m}''_T = S_T \rho_u. \tag{2.2}$$

The turbulent burning flux for a Re of 5,000 and 10,000 for jet-A flames are shown in Figure 2.11. Atmospheric (101 kPa) and sub-atmospheric (71 kPa) are open and closed symbols respectively. Again, labeled on Figure 2.11 are the two turbulence intensity cases (10 and 20%) that each have atmospheric and sub-atmospheric values. It is shown that the turbulent burning flux decreases as the pressure decreases for both Reynolds number conditions. This agrees with the work of Hui et al. [8] who showed that the laminar burning flux of jet-A increased with increasing pressure. This observations shows that, even under turbulent conditions, the mass burning flux behavior is similar to laminar conditions. As described previously, the laminar burning flux was affected by the increase in three-body termination reactions with an increase in pressure and the opposite was true for a decrease in pressure. Although the same may not necessarily true for the turbulent consumption speed, the argument can be made that there are similarities between the two. Under the proposed assumption, it can be concluded that turbulent consumption speeds are sensitive to changes in pressure by way of the effect of pressure on the unburned density.

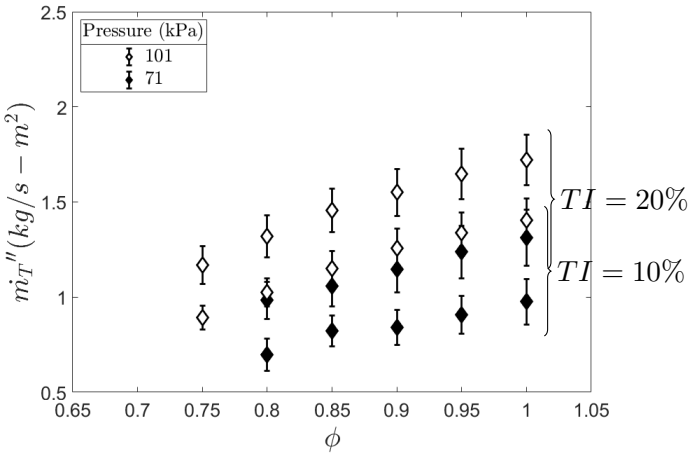

(a) Re of 5,000.

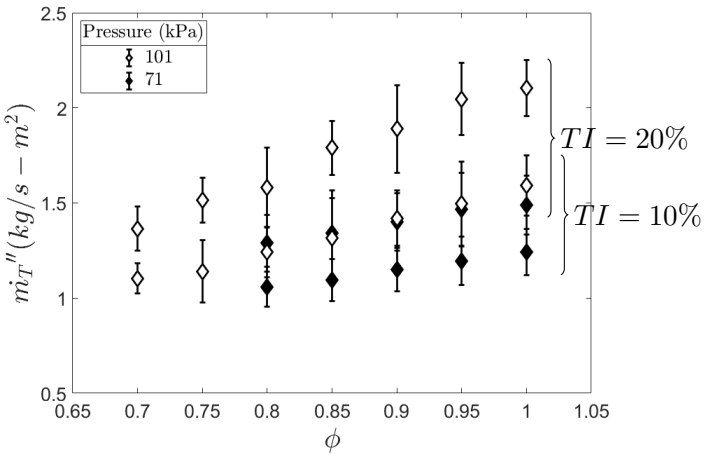

(b) Re of 10,000.

Figure 2.11: Turbulent burning flux values for jet-A at different equivalence ratios. C1 and C5 both exhibit similar behavior and have been omitted for clarity.

2.4.3 Stability

As noted previously, the flame front opened at sufficiently lean ϕ values. The last ϕ value just prior to the flame instabilities, or tip opening, is reported in table 2.3 for a Re of 10,000, turbulence intensity of 20%, and at atmospheric and sub-atmospheric pressures.

Table 2.3: Equivalence ratio (ϕ) at which the radial distribution showed tip quenching for pressures of 101 kPa and 71 kPa

	ϕ	
Fuel	Atmospheric (101 kPa)	Sub-atmospheric (71 kPa)
jet-A (A2)	0.65	0.78
ATJ Gevo (C1)	0.74	0.80
C10/TMB (C5)	0.72	0.78

At a pressure of 101 kPa, A2 had the greatest stability of the three fuels (e.g., tip opening at $\phi = 0.65$), while C1 is the least stable (tip opening at $\phi = 0.74$). As pressure reduced, tip opening is observed at higher equivalence ratios. For example, A2 and C5 experience tip opening at $\phi =$ 0.78, while C1 experiences tip opening at $\phi = 0.80$. Other research has shown that a decrease in aromatic content increases the stability of the flame front [8], [9], consistent with the trends observed for A2 and C5. In contrast C1 is made up of purely iso-alkanes, but a reduction in stability is seen. Fillo et al. [39] contributed the reduction in stability to the fact that C1 is more sensitive to turbulence induced stretch. It is possible that for C1 the sensitivity to turbulence induced stretch causing to flame tip to quench at higher ϕ values could be causing the pressure sensitivities seen between the three fuels. Other research has noted that adding iso- groups can make flames more prone to extinction [43]. It is possible, that the increase in methyl substitutions within iso- groups inhibits ignition and promotes extinction [44]. Furthermore, a decrease in stability from atmospheric to sub-atmospheric is seen between all fuels. This is attributed to a decrease in the flame brush thickness as pressure is reduced, increasing the limiting equivalence ratio at which the flame is stable [16], [19], [45].

2.5 Summary/Conclusions

Combustion behavior of jet-A and two jet-like fuels at two different pressures were compared using the turbulent consumption speed and the mass burning flux. The stability of these fuels at fuel-lean conditions was also reported. The measurements where taken of flames anchored to a turbulent Bunsen burner in an optically accessible pressure chamber. The turbulent consumption speed was dimensionally scaled by the zero-stretch laminar flame speed to discern turbulent sensitivities to pressure changes. The following conclusions were observed:

1. Turbulent consumption speeds of the three jet and jet-like fuels typically increased with decreasing pressure, depending upon the magnitude of the velocity fluctuations. This observation is counter to results reported previously for gaseous fuels. In contrast, normalized turbulent consumption speeds decreased with decreasing pressure, similar to trends reported for gaseous fuels.

2. The turbulent burning flux of jet-A, C10/TMB, and Gevo ATJ was shown to decrease with decreasing pressure, emphasizing the significant role that density has in controlling mass consumption rates.

3. Fuel chemistry of large hydrocarbon fuels can alter the susceptibility of turbulent combustion to changes in pressure. C1 (ATJ Gevo) was shown to be the most sensitive to pressure effects and flame tip opening consistent with previous work done [13]. This was attributed to C1's simple chemical make up (it being only a single component fuel) and due to lack of aromatic content within the fuel making the flame more sensitive to turbulence induced stretch.

4. Decreasing the pressure increased the propensity of the opening in the jet fuel flame tip. This is attributed to the thinning of the flame thickness by the increase in pressure gradients across the flame.

2.6 Supplementary Material

Supplementary data associated with this section can be found in appendix A. The supplementary data includes turbulent consumption speeds, mass burning fluxes, and radial profiles for determining stability for C1 and C5. Also included in this appendix is the calculated zero-stretched laminar flame speeds for A2, C1, and C5.

Chapter 3: Turbulent Combustion Behavior of a Surrogate Jet Fuel

Chapter 3 is an article that will be submitted for peer-review as a brief communication. The article focuses on the comparison of burning behavior of a surrogate jet fuel to burning of an industry standard fuel (jet-A). The article is adapted for the purposes of this thesis. The primary author of this article is the author of this thesis. The primary author provided most of the experimental setup, data collection, data analysis, and resulting conclusions from the data collected. Various co-authors provided help in experimental setup, data collection, and conclusions. The expected co-authors are as follows: Jonathan M. Bonebrake, Zohar Hoter, Aaron J. Fillo, and David L. Blunck.

3.1 Introduction

Jet fuels are made up of hundreds of different chemical constituents. This can be problematic when trying to model or test jet fuels because of the complexity of their composition. This situation makes surrogate fuels appealing because of their relatively simple composition for modeling and testing purposes [8], [9], [14]. Surrogate fuels are typically only made up of three constituents within four classes of fuels: an aromatic, n-alkane, iso-alkane, or a cyclo-alkane [23]. An understanding of how a surrogate fuel behaves in a combustion environment when compared to their more complex counterparts is needed to asses the usefulness of these fuels.

A parameter that is used commonly in literature for fuel comparison is the laminar flame speed [8], [9], [20]. The laminar flame speed is used because it is an indicator of the thermo-diffusive effects that are created by the chemical kinetics in the combustion process. For example, Kumar et al. [9] compared jet-A, an industry standard fuel, and S-8, synthetically derived jet fuel with similar thermophyiscal properties to jet-A. S-8 is a surrogate fuel entirely composed of n-alkanes and iso-alkanes [46]. The experimental results showed that jet-A and S-8 exhibit similar laminar flame speed results, thus showing similar flame propagation characteristics. A subsequent study done by Hui et al. [8] studied the pressure effects on the burning behavior of jet-A and S-8. It was found that both fuels had similar flame speeds and laminar burning fluxes from pressures ranging from 1 to 5 atmospheres.

Little research has been performed on the effects of turbulence on the combustion process of surrogate fuels [47]. Not considering combustion behavior of surrogate fuels in a turbulent environment is potentially problematic because flow conditions in a typical combustor are highly turbulent [11]. A parameter that can be used to discern turbulent combustion effects is the turbulent consumption speed [18]–[20]. The turbulent consumption speed is a metric that is influenced by both the chemical kinetics and turbulence characteristics [17]. The turbulent consumption speed is also useful for closure models of mean reaction rates in turbulent combustion modeling and can be used for validation of these models [20], [48].

With this background and motivation, the objective of this study is to identify similarities and differences of the burning behavior of a 3-component surrogate fuel to a fuel commonly used in industry, jet-A, in a turbulent combustion environment. The surrogate fuel is of interest because the combustion behavior is not well understood, especially in a turbulent combustion environment [23].

3.2 Methodology

3.2.1 Experimental Setup

The experimental arrangement for conducting the turbulent consumption speed measurements is illustrated in Figure 3.1 and includes a fuel vaporizer, Bunsen burner, and a pressure chamber. The Bunsen burner configuration was based on the design developed by Venkateswaran et al. [33]. A Thermal mass flow meter and a syringe pump metered the air and fuel, respectively. The fuel was injected through a siphon air-atomizing nozzle into the vaporizer, where it mixed with the incoming air. The fuel/air mixture was heated to temperatures near 475 K within the vaporizer. The mixture flowed through a turbulence generator inside the Bunsen burner. At the exit of the burner, a premixed methane/air flame ignited the mixture and anchored the jet to the burner. The Bunsen burner's flame was contained within an optically accessible pressure chamber. The experimental arrangement allowed for control over the Reynolds number of the flow, the equivalence ratio or the ratio of fuel-to-air in the mixture (ϕ), the turbulence intensity (TI), and the pressure. Fuel flow rates, Reynolds numbers, and fuel-to-air ratios where calculated using fluid properties provided by EES, see appendix D.

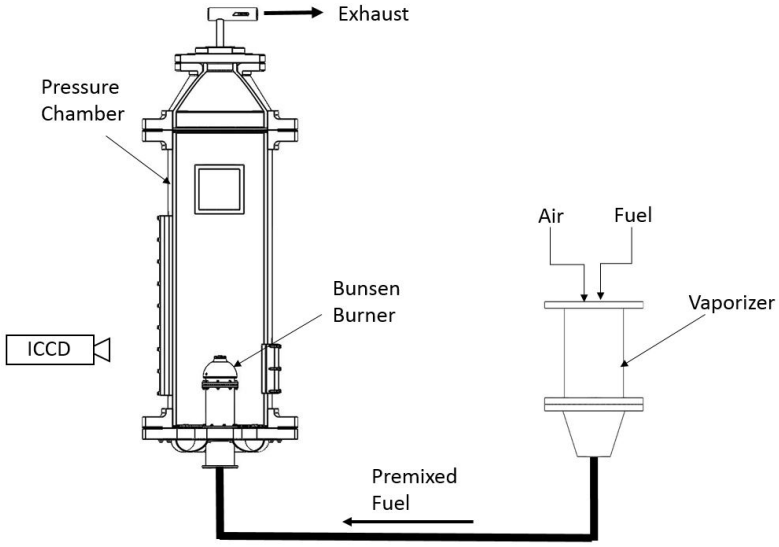

Figure 3.1: Schematic of the turbulent Bunsen burner and vaporizer.

The fuel types examined were jet-A (a conventional jet fuel) and a surrogate fuel. Table 3.1 lists the thermophysical properties of the two jet fuels. The similarities in the lower heating value is important because the flame speed is often sensitive to temperature [8], [16], [18], [19]. Similar lower heating values will provide similar flame temperature helping control the sensitivity to temperature. The surrogate fuel is made up of three large hydrocarbon chains: n-dodecane, iso-octane and 1,3,5 trimethyl benzene (59.3, 18.4 and 22.2 % vol respectively). Table 3.2 lists distribution of aromatics, alkanes, etc. within the two fuels. Note that A2 does not add up to 100% because of other additives within the fuel. Both fuels were tested at a Reynolds numbers of 10,000, a turbulence intensity of 20%, and at pressures of 101 kPa and 71 kPa (atmospheric and sub-atmospheric respectively). These conditions were chosen because they were the upper (lower) limits of the testing apparatus.

Table 3.1: Thermophysical properties of the surrogate and jet-A [23].

Fuel	Average Molecular Formula	Lower Heating Value (MJ/kg)	Molecular Weight (g/mol)	Density (kg/m^3)
jet-A (A2)	$C_{11.4}H_{21.8}$	43.06	159	0.803
Surrogate (S1)	$C_{10.3}H_{20.1}$	42.92	156.9	0.769

Table 3.2: Composition of three chemical compound chains of the surrogate and jet-A [23].

Fuel Designation	Aromatics (% vol)	iso-Alkanes (% vol)	n-Alkanes (% vol)
jet-A (A2)	11.2	39.1	27.2
Surrogate (S1)	22.2	18.4	59.3

3.2.2 Data Analysis

Turbulent Consumption Speed

An Andor Solis ICCD camera was used to measure the chemiluminescence of the turbulent Bunsen flame. Three sets of 360 images were taken of the flame at a rate of 2 kHz. The 360 images were averaged to obtain the average flame brush. The flame brush area was calculated for the definition of the turbulent consumption speed with the following equation [17],

$$S_T = \frac{\dot{m}}{A_{\langle c \rangle} \rho_u}. \tag{3.1}$$

Here $\dot{m}$ is the mass flow rate, $A_{\langle c \rangle}$ is the time averaged area of flame brush, and ρ_u is the unburned density. The calculation of the mean cone area of the flame was adapted by Fillo et al. [39]. Details involving this process is explained in previous works and in section 2.3.2 [39], [49]. The turbulent burning flux ($\dot{m}''_T$) was also calculated from the turbulent consumption speed and is defined as,

$$\dot{m}''_T = S_T \rho_u. \tag{3.2}$$

Stability

The approach described in section 2.3.2 was used to determine the stability of the two jet fuels. A brief summary of the approach is described here. Using a Phantom veo 710 high speed camera, emissions from the flame was captured for a range of equivalence ratios, ranging from stable to unstable. By averaging a set of 16,000 images taken at 8 kHz, an average image was created to determine the equivalence ratio (ϕ) at which the flame becomes unstable. The flame became unstable when the tip of the Bunsen flame quenched and fuel passed through the flame without

igniting. Quenching of the tip was shown by slicing a radial profile at the maximum intensity location of the average image. The flame is classified as unstable when either a biomodal distribution forms from the radial profile or a sharp decrease in intensity towards the middle of the flame (r = 0), than a gradual decrease. These distributions form because the maximum intensity shifts to the fringes of the flame.

3.3 Results

Figure 3.3a is the turbulent consumption speeds for A2 and S1 at atmospheric pressure. A2 and S1 have statistically similar turbulent consumption speed values at atmospheric conditions. Figure 3.3b is the turbulent consumption speeds for A2 and S1 at sub-atmospheric pressure. As seen in figure 3.3b, both fuels have a 5 to 15% increase in consumption speed as pressure decreased and have similar sensitives to reduce pressure. Figure 3.2 shows the turbulent burning flux determined from the turbulent consumption speed. Similar to consumption speed results, S1 and A2 are statistically similar to each other, emphasizing the similarities between the two fuels, even when pressure changes.

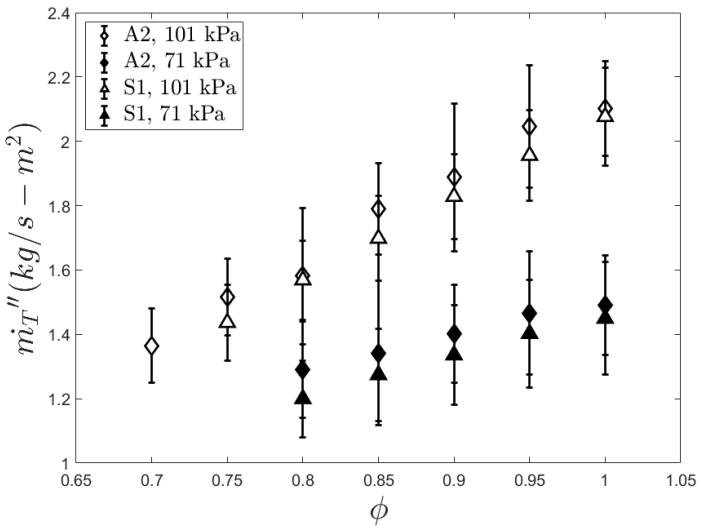

Figure 3.2: Turbulent burning flux of jet-A and the surrogate fuel at a Re of 10,000 and a turbulence intensity of 20%.

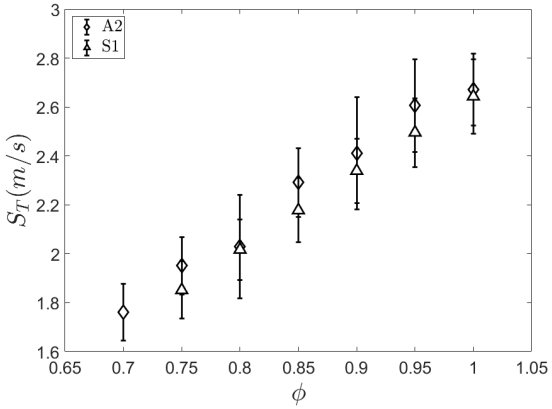

(a) Turbulent consumption speeds of jet-A and the surrogate fuel at atmospheric conditions (101 kPa).

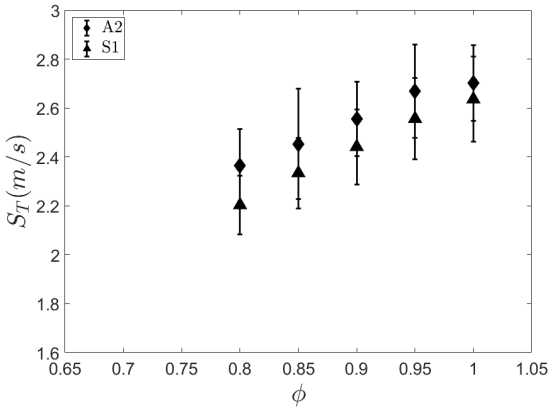

(b) Turbulent consumption speeds of jet-A and the surrogate fuel at sub-atmospheric conditions (71 kPa).

Figure 3.3: Turbulent consumption speeds of jet-A and the surrogate fuel at a Re of 10,000 and a turbulence intensity of 20%.

The sensitivity of the two fuels to tip opening was evaluated by the radial distributions shown in Figure 3.4. The ϕ value at which tip opening is determined is shown as a sharp decrease near r = 0 or by the appearance of a biomodal distribution. It is shown that at atmospheric conditions, A2 is more stable (ϕ = 0.70) than S1 (ϕ = 0.76). This is consistent with other work showing that a decrease in aromatic content leads to a increase in stability [8], [15], [39]. However, at sub-atmospheric pressure, the stability of the two fuels are similar (ϕ = 0.80). It has been shown

that for gaseous fuels that the stability of the Bunsen tip is dominated by turbulent eddies over thermal-diffusive effects [34]–[36]. This is not evident in the atmospheric case because of the differing stability with varying chemical compositions, but the stability of these fuels are the same at the sub-atmospheric case. This could possibly be due to an increase in the effect of turbulence induce stretch on the flame front under reduced pressures.

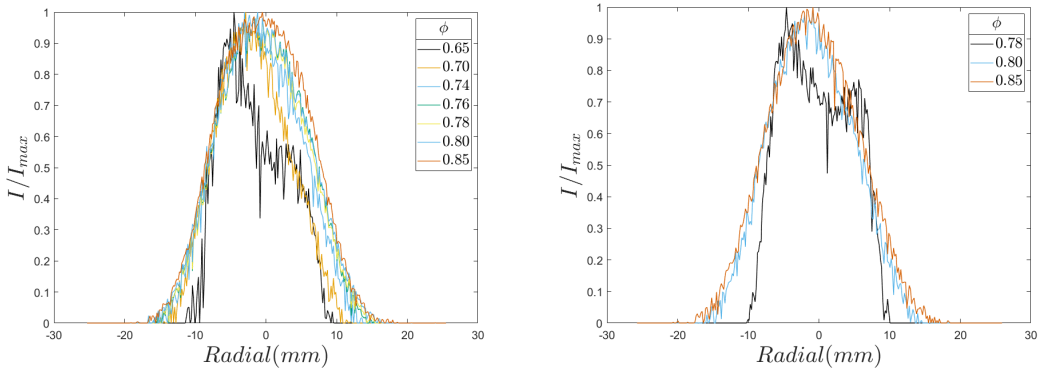

(a) A2 at 101 kPa.

(b) A2 at 71 kPa.

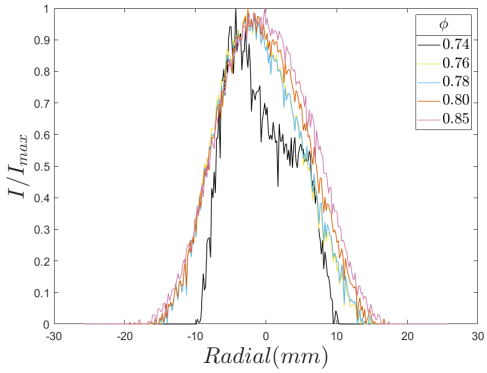

(c) S1 at 101 kPa.

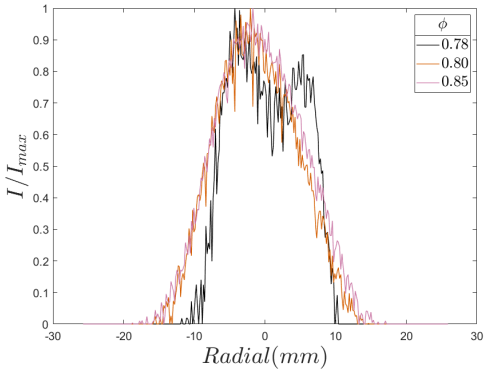

(d) S1 at 71 kPa.

Figure 3.4: Radial profiles for A2 and S1 at the maximum intensity location. The curve representing instabilities is denoted as a black line.

3.4 Summary/Conclusions

In this work, the combustion behavior of a 3-component surrogate, made up of n-dodecane, iso-octane, and 1,3,5 trimethyl benzene, and jet-A, a fuel used commonly in industry, where

compared on a turbulent Bunsen flame. It was shown the A2 and S1 have similar flame propagation in the turbulent regime even with varying chemical compositions. This was proven by statistically similar turbulent consumption speeds and turbulent burning fluxes. This shows that matching key fluid properties (e.g., density and lower heating values) could allow for similar combustion behavior. However, A2 showed greater stability then S1 at atmospheric pressures potentially due to the increased aromatic content. However, at sub-atmospheric pressure A2 and S1 showed similar stability. This could be due to an increase in the turbulence induced stretch on the flame tip under reduced pressures.

Chapter 4: Summary and Future Work

4.1 Summary/Conclusions of Work

Combustion behavior of jet-A and three jet-like fuels at two different pressures was compared using the turbulent consumption speed and the turbulent burning flux. Turbulent consumption speed and the turbulent burning flux were determined from measurements of piloted turbulent Bunsen flames contained within a pressure vessel. The following conclusions were observed:

1. Turbulent consumption speeds of large hydrocarbon fuels increased on average with decreasing pressure, which is in contradiction with work done on the turbulent combustion of gaseous fuels. However, when normalized by the zero-stretch laminar flame speed, in specific regions, the normalized turbulent consumption speed decreased with decreasing pressure, which is similar to work done on the turbulent combustion of gaseous fuels.

2. The turbulent burning flux for the jet fuels decreased with decreasing pressure, emphasizing the importance of the reactant density on the turbulent consumption speed. This was in agreement with other work reported for the laminar burning flux, emphasizing the similarities between laminar and turbulent combustion.

3. Fuel chemistry of large hydrocarbon fuels can alter the susceptibility of turbulent combustion to changes in pressure. In this work, C1 (ATJ Gevo) was found to be the most sensitive to pressure effects and lean combustion effects. This was attributed to C1's simple chemical make up (it being only a single component fuel) and due to lack of aromatic content within the fuel.

4. Decreasing the pressure increased the propensity of the opening in the jet fuel flame tip. This is attributed to the thinning of the flame thickness by the increase in pressure gradients across the flame.

5. It was found that the turbulent consumption speeds of a simple 3-component surrogate and jet-A are statistically similar at various equivalence ratios and pressures. This shows

that the chemical kinetics are similar between the two fuels under turbulent pre-vaporized conditions.

6. The simple surrogate had a lower stability limit than A2. The lower stability is contributed to the lack of other hydrocarbon components that are present in A2 but not the surrogate.

4.2 Suggested Future Work

The conclusions stated can be further explored by several supplemental studies. The suggested studies are as follows:

1. Evaluating the effects of higher $(P/P_0)(u'/S_{L,0})$ ratios in sub-atmospheric environment. This can be accomplished by increasing the turbulent fluctuations (u') by increasing the Reynolds number of the flow.

2. Fully evaluating the turbulent combustion velocity field. 1-D hot wire measurements of the flow velocity where compared to 3D measurements done by Marshall et al. [30] and showed good agreement [13]. However, expanding the measurement from a 1D to 3D measurement can greatly enhance the scaling of the turbulent consumption speeds. This can be accomplished by several techniques; 3D hot wire anemometery by use of a 2-wire probe or by laser doppler velocimetry [50], [51].

3. Exploring the stability limits at other flow and turbulent conditions. The conditions reported in this paper were for only one Reynolds number and one turbulence intensity. It would be advantageous to see how differing flow characteristics and turbulent fluctuations effect the stability of the fuels tested.

4. Analyzing local pocket formation (an absence of combustion) within the flame front to discern stability effects on the turbulent consumption speed. Local pocket formation forms due to the generation of vortices within the turbulent flame front. It is hypothesized that the reason for higher differences between atmospheric and sub-atmospheric values for lower equivalence ratios is caused by localized opening within the flame front. This was explored by analyzing pocket formation in the flame, but was excluded from the research focus of this paper as it was outside of the scope and incomplete. For more information regarding the method and the preliminary results, please see appendix B.

5. Expanding the flow conditions of the surrogate turbulent consumption speed data. The flow conditions could include varying the Reynolds number and turbulent intensity. It would be advantageous to calculate the zero-stretch laminar flame speed of the surrogate fuel for use in dimensionally scaling the turbulent consumption speed values to determine turbulent and pressure sensitivities.

APPENDICES

Appendix A: Supplemental Figures

Turbulent consumption speed, turbulent burning flux and radial distributions for C10/TMB and ATJ Gevo are included for further reference. Also included in this appendix is the zero stretch laminar flame speed data provided for this studies use by Dr. Hai Wang'ss group from USC.

A.1 Supplemental Data for C1 (ATJ Gevo)

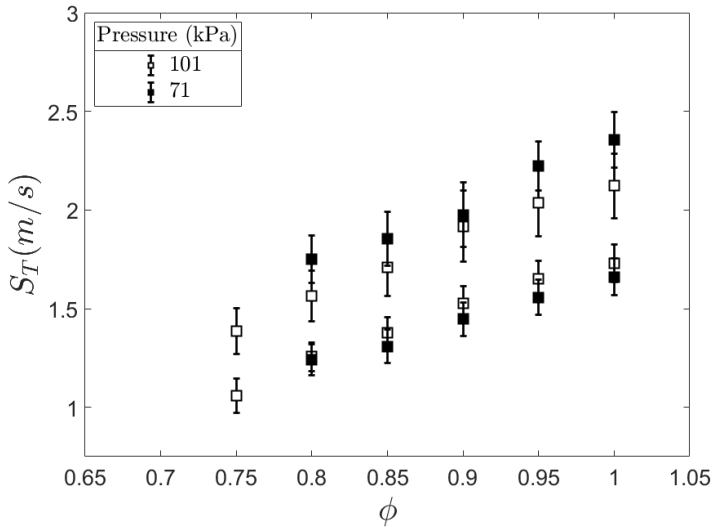

Figure A.1: Turbulent consumption speed values for ATJ Gevo at a Re of 5,000 and at different equivalence ratios.

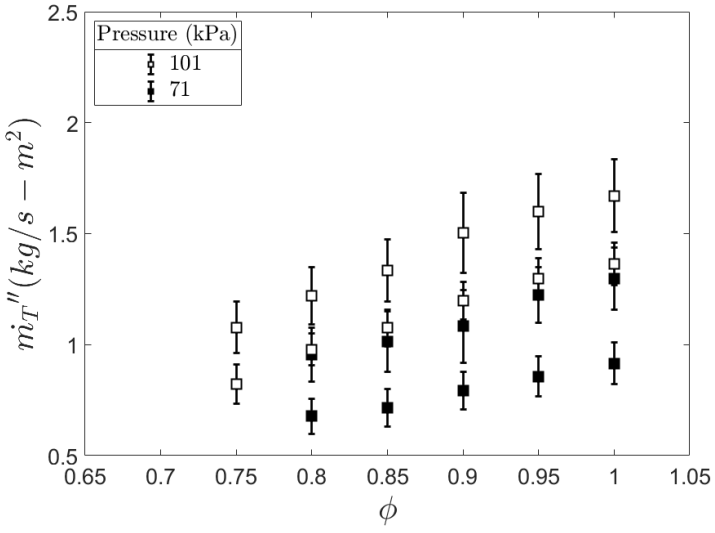

(a) Re of 5,000.

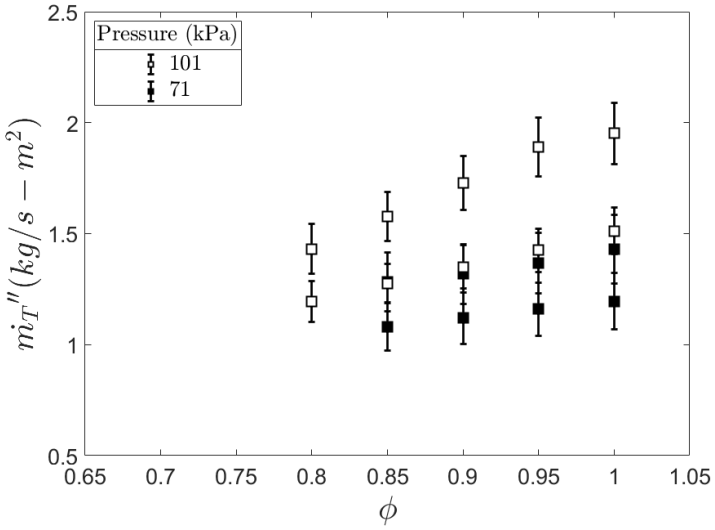

(b) Re of 10,000.

Figure A.2: Turbulent burning flux values for ATJ Gevo at different equivalence ratios.

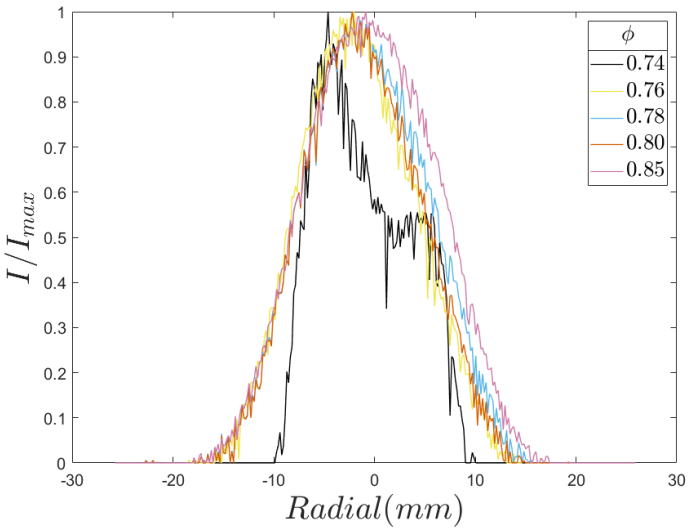

(a) C1 stability curves at 101 kPa.

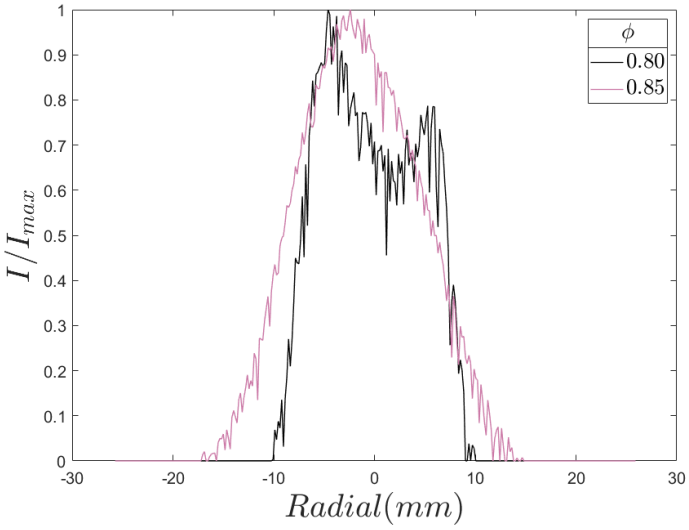

(b) C1 stability curves at 71 kPa.

Figure A.3: Radial profiles for ATJ Gevo. The curve representing instabilities is denoted as a black line.

A.2 Supplemental Data for C5 (C10/TMB)

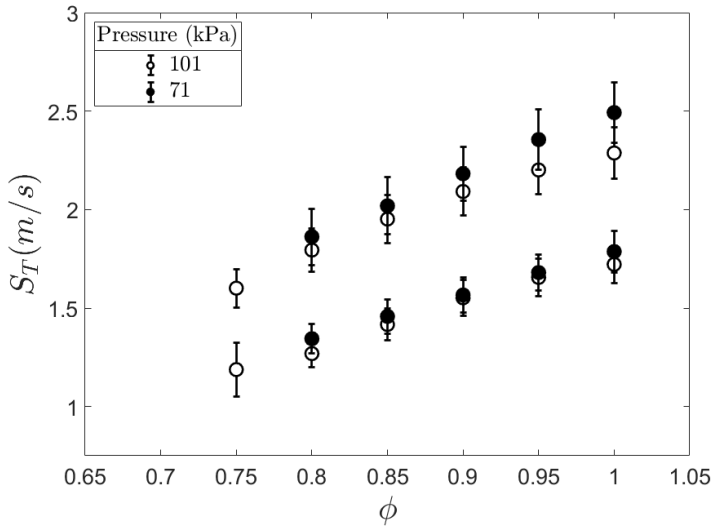

Figure A.4: Turbulent consumption speed values for C10/TMB at a Re of 5,000 and at different equivalence ratios.

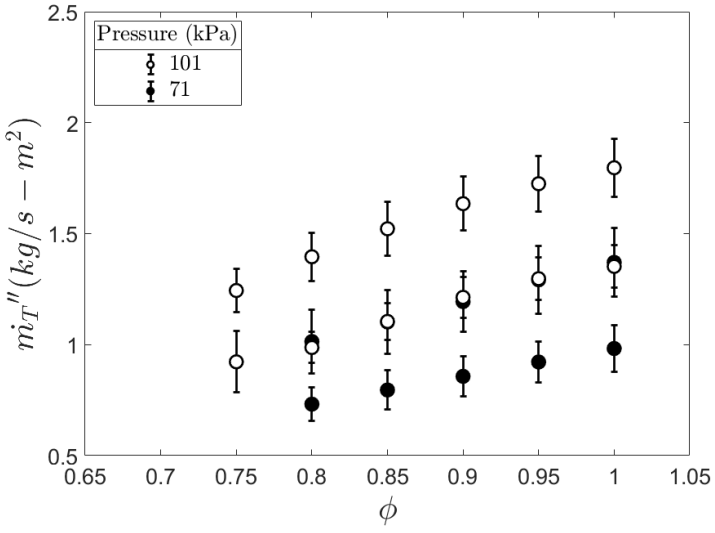

(a) Re of 5,000.

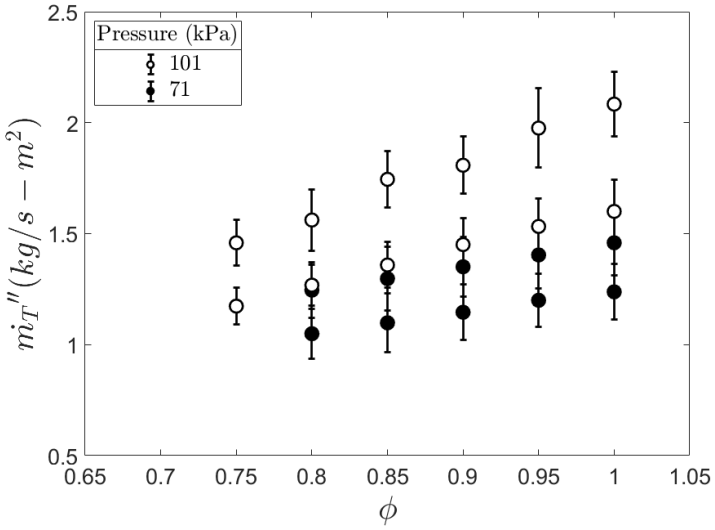

(b) Re of 10,000.

Figure A.5: Turbulent burning flux values for C10/TMB at different equivalence ratios.

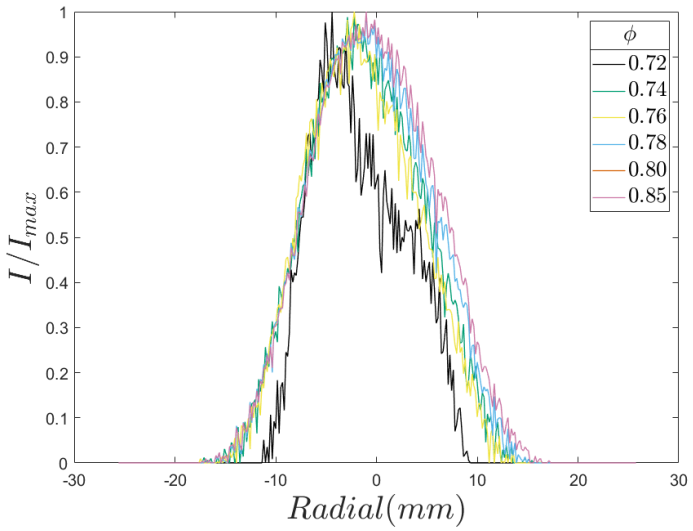

(a) C5 stability curves at 101 kPa.

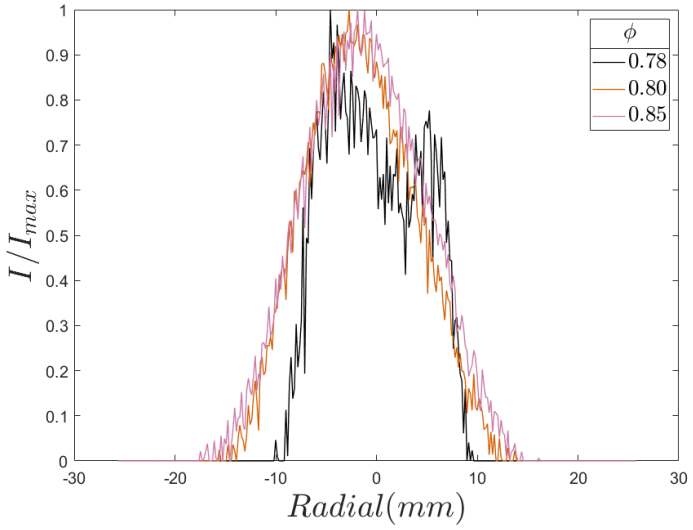

(b) C5 stability curves at 71 kPa.

Figure A.6: Radial profiles for C10/TMB. The curve representing instabilities is denoted as a black line.

A.3 Zero-Stretch Laminar Flame Speeds

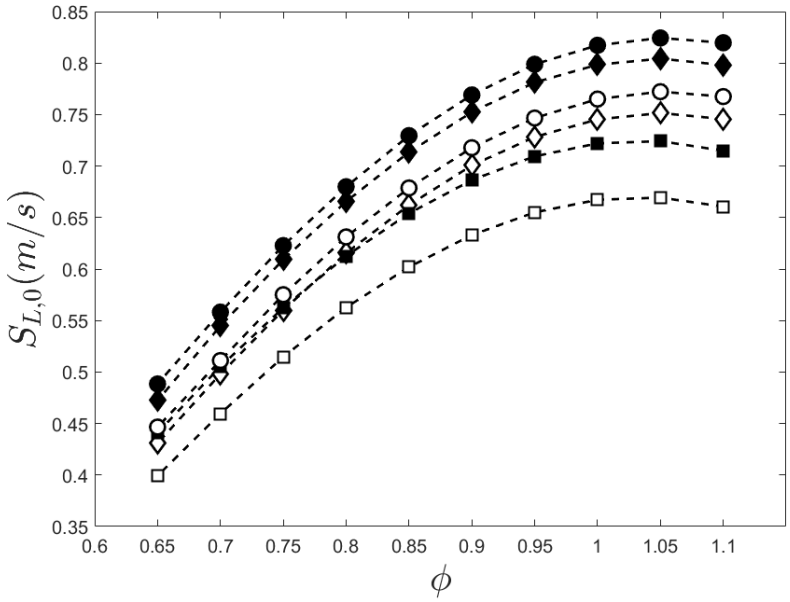

Figure A.7: Zero-stretch laminar flame speeds for A2, C1, and C5.

.

Appendix B: Pocket Analysis Method and Preliminary Results

Described in Appendix is the process for determining pockets within the flame front and preliminary results. By binarizing each of the high speed images, pockets can be detected within the flame front. The Otsu thresholding method [52] was used for the binarization process as it gave the best results. To eliminate any artificial pockets that where created during the binarzation, the image was eroded then dilated [53]. Lastly, boundaries where traced along the edges of the binarized image for determining the number of pockets, pocket area, and total flame area [54].

B.1 Pocket Determination Process

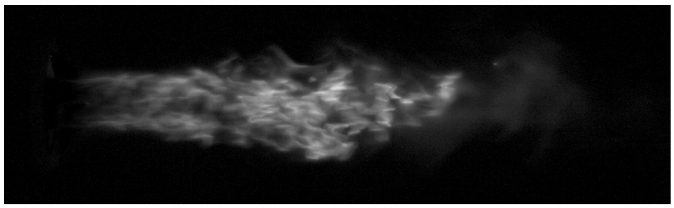

(a) Instantaneous image of jet-A flame.

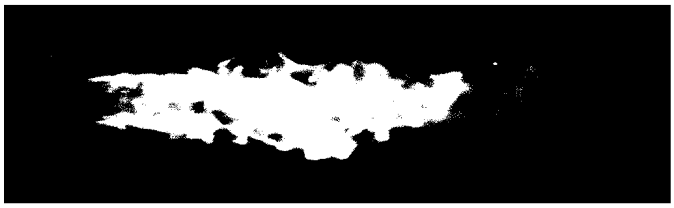

(b) Binarized image using the Otsu method.

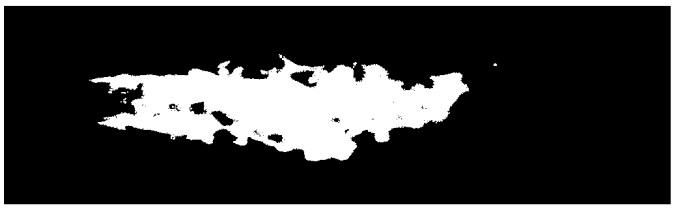

(c) Erosion and dilation of the binarized imaged using 2-by-2 square structural element [55].

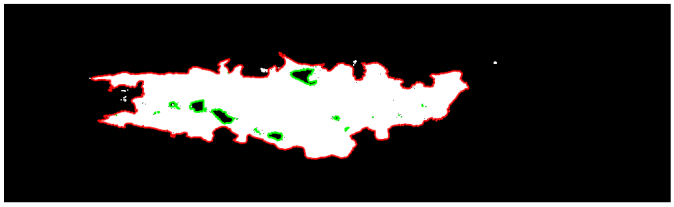

(d) Traced edges of the pockets (green) and the outer edge of the flame (red).

Figure B.1: Processing steps for detecting the edges of the flame and pockets from top to bottom. Flame images depicted are at Reynolds number of 10,000 and a TI of 20%.

B.2 Preliminary Results

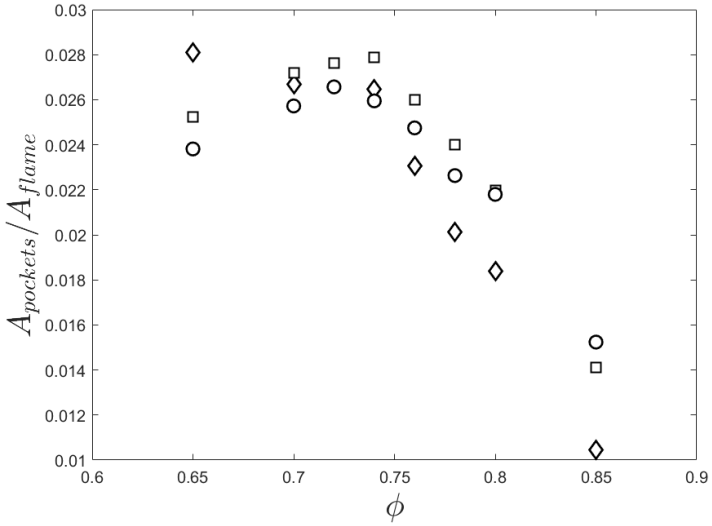

(a) Pocket data taken at 101 kPa.

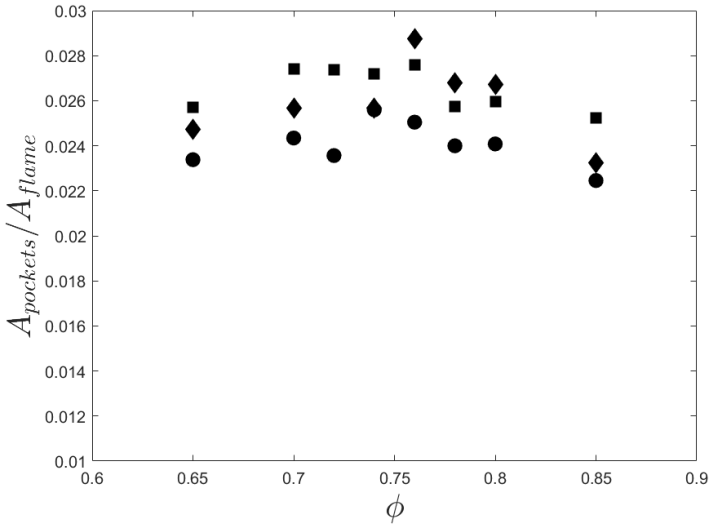

(b) Pocket data taken at 71 kPa.

Figure B.2: Equivalence ratio (ϕ) compared against the ratio of pocket area and flame area. Data taken at a Re of 10,000 and turbulence intensity of 20%.

Appendix C: Uncertainty Analysis

A more detailed uncertainty analysis is described in the work done by Fillo [13], but a brief description is described here. The uncertainty for the turbulent flame speeds was calculated using the Kline-McClintock method, sequential perturbation, and statistical methods. The Kline-McClintock method was used to calculate the instrument uncertainty and data analysis (U_{Bias}). Sensitivity to the pilot flame was calculated using sequential perturbation by varying the heat release ratio of pilot flame and the main jet flame (U_{Pilot})(the best ratio was found to be about 10%). A student-t distribution was applied to the turbulent consumption speed values with a 95% confidence interval for the precision uncertainty (U_P). On average, every equivalence ratio at each condition has 6 to 10 data points. The total uncertainty for the turbulent consumption speed was calculated by the root sum of the squares described as follows,

$$U_{S_T} = \sqrt{U_P^2 + U_{Bias}^2 + U_{Pilot}^2}. \tag{C.1}$$

C.1 Estimated Uncertainty Values

Table C.1: Estimated uncertainty on the turbulent consumption speed.

Variable	% Uncertainty
U_P	6-8%
U_{Bias}	$\sim$2%
U_{Pilot}	$\sim$5%
U_{S_T}	$\sim$6-8%

Appendix D: Flow Rate Equations and Definitions (EES)

Flow rate calculations for Jet-A (A2)

Refrence States

$T_{ref} = 273$ [K]

$P_{ref} = 101.325$ [kPa]

$R = 8.314$ [kJ/kmol-K] $\cdot \left| 0.001 \cdot \frac{\text{kJ/mol–K}}{\text{kJ/kmol–K}} \right|$

Molecular Weight

$MW_{air} = \textbf{MolarMass}(\text{Air}) \cdot \left| 1 \cdot \frac{\text{g/mol}}{\text{kg/kmol}} \right|$

$MW_{fuel} = 159$ [g/mol] *Molecular weight of A2*

Stoichometric balance of air and fuel mixture, Turns Page 21

$x = 11.4$ *Carbon amount when balancing ideal combustion case, see Turns Page 21*

$y = 22.1$ *Hydrogen amount when balancing ideal combustion case, see Turns Page 21*

$a = x + \frac{y}{4}$ *Total Air amount when balancing ideal combustion case, see Turns Page 21*

Air to Fuel ratio

$AF = 4.76 \cdot \frac{a}{\phi} \cdot \frac{MW_{air}}{MW_{fuel}}$ *Calculating Air-to-Fuel ratio based on equivlance ratio (phi) given*

Total Mass flow rate

$d = 12$ [mm] $\cdot \left| 0.001 \cdot \frac{m}{mm} \right|$ *Diameter of Jet*

$\dot{m}_{total} = \pi \cdot \textbf{Visc}(\text{Air}, T = 473 \text{ [K]}) \cdot Re \cdot \frac{d}{4}$ *Calculating total mass flow rate at 200 degrees C based off of the Reynolds number set by the user assuming ideal gas*

Mass Fraction of air

$Y_{air} = \frac{AF}{AF + 1}$ *Calculating the mass fraction of air based off of the fuel-to-air ratio*

Mass Fraction of Fuel

$Y_{fuel} = 1 - Y_{air}$ *Calculating the mass fraction of fuel based off of the fuel-to-air ratio*

Mass flow rates of fuel and air

$\dot{m}_{air} = Y_{air} \cdot \dot{m}_{total}$ *Calculating the mass flow rate of air based off of the mass fraction air*

$\dot{m}_{fuel} = Y_{fuel} \cdot \dot{m}_{total}$ *Calculating the mass flow rate of fuel based off of the mass fraction fuel*

Volumetric flow rate of fuel and air

$\rho_{ASTM,A2} = 803$ [kg/m^3] *ASTM Density of A2*

$Main_{Air} = \dot{m}_{air} \cdot \mathbf{v}(Air, T = T_{ref}, P = P_{ref}) \cdot \frac{300}{250} \cdot \left| 60000 \cdot \frac{L/min}{m^3/s} \right|$ *Calculating the volumetric air input for the mass flow controllers at 0 degree C reference temperatures*

$Fuel_{Pump} = \dot{m}_{fuel} \cdot \frac{1}{\rho_{ASTM,A2}} \cdot \frac{\left| 6 \times 10^7 \cdot \frac{mL/min}{m^3/s} \right|}{2}$ *Calculating the volumetric fuel input for the syringe pumps at 0 degree C reference temperatures*

Pilot Heat Release Calculations

$LHV_{ASTM,A2} = 43.06$ [MJ/kg] $\cdot \left| 1000 \cdot \frac{kJ/kg}{MJ/kg} \right|$ *Lower heating value for A2*

$\dot{Q}_{fuel} = \dot{m}_{fuel} \cdot LHV_{ASTM,A2}$ *Calculating the heat generated from the fuel*

$\dot{Q}_{CH4} = \dot{m}_{CH4} \cdot \mathbf{LowerHeatingValue}(CH4)$ *Calculating the heat generated from the methane pilot flame*

$\frac{\dot{Q}_{CH4}}{\dot{Q}_{fuel}} = 0.115$ *Setting the ratio of the heat generated from the methane flame and fuel to 11.5%, see Aaron Fillos thesis for more information*

Volumetric Flow rate of CH4

$Pilot_{Methane} = \dot{m}_{CH4} \cdot \mathbf{v}(CH4, T = T_{ref}, P = P_{ref}) \cdot \left| 60000 \cdot \frac{L/min}{m^3/s} \right|$ *Calculating the volumetric methane input for the mass flow controllers*

Mass flow rate of Pilot Air

$MW_{CH4} = \mathbf{MolarMass}(CH4) \cdot \left| 1 \cdot \frac{g/mol}{kg/kmol} \right|$

$AF_{pilot} = 4.76 \cdot 2 \cdot \frac{MW_{air}}{MW_{CH4}}$ *Calculating the air-to-fuel ratio for the methane flame based on a stoichmetric mixture of methane to a r*

$\dot{m}_{pilot,air} = AF_{pilot} \cdot \dot{m}_{CH4}$ *Calculating the mass flow rate of the pilot air based off of the air-to-fuel ratio*

Volumetric flow rate of Pilot Air

$Pilot_{Air} = \dot{m}_{pilot,air} \cdot \mathbf{v}(Air, T = T_{ref}, P = P_{ref}) \cdot \left| 60000 \cdot \frac{L/min}{m^3/s} \right|$ *Calculating the voulmetric pilot air input for the mass flow controllers*

MW of entire Mixture

$MW_{mix} = \frac{1}{\frac{Y_{air}}{MW_{air}} + \frac{Y_{fuel}}{MW_{fuel}}}$

Total molecular weight of the mixture, see Turns page 21

Percentage of Fuel and Air within Mix

$$X_{fuel} = \frac{MW_{mix}}{MW_{fuel}} \cdot Y_{fuel}$$ *Calculating the mass percantage of fuel*

$$X_{air} = \frac{MW_{mix}}{MW_{air}} \cdot Y_{air}$$ *Calculating the mass percantage of air*

Density of the fuel at nozzle exit temperature

$$\rho_{fuel} = P_{ref} \cdot P_{chamber} \cdot \frac{MW_{fuel}}{R \cdot T_{nozzle,exit}}$$ *Calculating the density of the fuel assuming it is an ideal gas at the ambiet pressure, user can control chamber pressure for desired density*

Unburned density

$$\rho_u = X_{fuel} \cdot \rho_{fuel} \cdot \left| 0.001 \cdot \frac{kg/m^3}{g/m^3} \right| + X_{air} \cdot \rho\left(Air, T = T_{nozzle,exit}, P = P_{ref} \cdot P_{chamber}\right)$$ *Calculating the density of the unburned mixture*

Appendix E: Processing Code

Provided in this appendix is the image processing code calculating the mean flame area that was adapted from Fillo [13]. Also included in this appendix is the processing code for calculating the radial profiles for determining tip opening and the pocket analysis code. Flow rate calculations are included in this appendix that were adapted from Fillo.

E.1 Flame Area Calculation (MATLAB)

```
clear
clc
close all

Codepath = 'D:\Flame Speed\AbelTransformCodes_OSU\Old Code';
Datapath = 'D:\Flame Speed\Raw Tiff Files\2019\Apr\04-05-2019';
bg_path = 'D:\Flame Speed\Raw Tiff Files\2019\Apr\04-05-2019\
    background.tiff';
Cal_path = 'D:\Flame Speed\Raw Tiff Files\2019\Apr\04-05-2019\
    calibration.tiff';
fg_path = 'D:\Flame Speed\Raw Tiff Files\2019\Apr\04-05-2019\
    f01.tiff';

%% Input Parameters
m_dot_total = 0.001214;
rho_u    = 0.7874;
D        = 12;                          %Burner Diameter

%% Image Parameters - Selected From Image
flame_img = imread(Cal_path);

```

```
19 figure
20 imshow(flame_img)
21 colormap('Bone')
22 axis image
23 title('Select Left edge, Right Edge, Bottom')
24 [x_flame,y_flame] = ginput(3);
25 Lf                          = x_flame(1);
                                                % left edge of the
    flame
26 Rf                          = x_flame(2);
                                                % right edge of the
    flame
27 Bcrop                       = y_flame(3);
                                                 % location for
    cropping of the top of the image
28
29 imshow(flame_img)
30 colormap('bone')
31 axis image
32 title('Select Left edge, Right Edge of calibration device')
33 [x_cal,y_cal] = ginput(2);
34 Left                        = x_cal(1);
                                                % location of left
    line on calibration device
35 Right                       = x_cal(2);
                                                % location of right
    line on calibration device
36
37 %% Some constants for picking out the pixels, you can use
    these to
38 % manually pick out pixels
39 %
40 % Lf = 414;
```

```
41 % Rf = 607;
42 % Left = 417;
43 % Right = 588;
44
45 %% Image Parameters - User Selected
46 %Comment out Lf Rf Bcrop Tcrop Length Right and Left for
       spacial
47 %calibration determination
48
49 C                       = (Lf + Rf)/2;
                                        % center of burner
50 diameter                = 0.012;
                                                          %
       use if no calibration image
51 pixels                  = Right - Left;
52 Calibration             = 0.03/pixels;
                                        % meters/pixel, based
       off 1 cm calibration length
53 Tcrop                   = 1;
                                              % pixel
       location of the burner lip: y-location
54 R                       = 0.008;
55
56 C = 512;
57
58 %% Calibration Heigth Correction
59 beta = 0.00655/Calibration;
60
61 Bcrop = Bcrop + beta;
62
63 % Bcrop = 973;
64
65 %% Calculate radius and volume flow rate
```

```
% Change to volumetric flow rate from data
% USE MASS FLOW AND UNBURNED DENSITY

r                           = (D/2)*10^-3;
                                        % burner radius (m)
v_dot                       =  m_dot_total/rho_u;
                                % volume flowrate (m^3/s)

%% Image Read In, Average, and Background Subtract
% add for loop to repeat for number of runs as needed.
info = imfinfo(fg_path);
num_images = numel(info);
for i = 1:360
    fg_image(:,:,i) = imread(fg_path,i,'Info',info);
    bg_image(:,:,i) = imread(bg_path,i,'Info',info);
end

MeanImg = mean(fg_image,3);
Mean_bg = mean(bg_image,3);
BG_sub = MeanImg-Mean_bg;
BG_sub(BG_sub < 0) = 0;

figure
image(BG_sub)
%% Image crop dimensions
[ydim, xdim, cases] = size(MeanImg);

Lcrop                       = floor(C - (1/Calibration)*R);
                    % location for cropping on left side of
    image (0.5 cm from OD of burner lip)

if Lcrop < 1
    error('Cropping domain is larger than actual image');
```

```
95  end
96
97  Rcrop                       = floor(C + (1/Calibration)*R);
                        % location for cropping on right side of
       image (0.5 cm from OD of burner lip)
98  if Rcrop > xdim
99      error('Cropping domain is larger than actual image');
100 end
101
102 ImCrop = BG_sub(ceil(Tcrop):ceil(Bcrop), ceil(Lcrop):ceil(Rcrop
       ));          % crop the image
103 Intensity  = ImCrop;
104
105 figure
106 image(ImCrop)
107 axis image
108 %% Axisymmetrize the image by averaging both sides
109
110 Axisym = 0.5*(Intensity(:, 1:end) + Intensity(:, end + 1 - (1:
       end)));
111 [f, g] = size(Axisym(:, :));
                                                    % get dimensions
       of the axisymmetrized image
112
113 %% Perform median filter on images
114
115 ImageFilt(:, :) = medfilt2(Axisym(:, :), [5 5]);
116
117 %% Extract the centerline intensity of the filtered axisym
       image
118
119 CL_axisym = zeros(f,1);
120 CL_axisym(:) = ImageFilt(:, round(g/2));
```

```
121 CL_axisym = flipud(CL_axisym);
122
123 %% Perform the Abel Transform to each image
124
125 ImageAbel(:, :) = abeltransform(ImageFilt(:, :));
126
127 %% Create array of centerlines for each Abel transformed image
128
129 CL = zeros(f,1);
130 CL(:) = ImageAbel(:, round(g/2));
131 CL = bwfilter(CL, 1 : length(CL), 0.01);
132 CL = flipud(CL);
133
134 %% Fit Gaussian to each centerline and find maximum location
135
136 GF          = zeros(f,1);
137 H           = zeros(1);
138 ft          = fittype('gauss1');
139 options     = fitoptions('gauss1');
140 pxl         = (1:f)';
                                                        %
    create pixel location vector
141 met         = pxl*Calibration;
                                                  % convert pixel
     location vector into meters
142 curvefit    = fit(pxl, CL(:), ft, options);
                                        % create fit model
143 GF(:)       = curvefit(pxl);
                                                    % evaluate
    fit model for pixel vector
144 [GFmax, I]  = max(GF(:));
                                                        % find the
     magnitude and location of the maximum value of the Gaussian
```

```
145 H            = I*Calibration;
                                                    % convert the
      location of the maximum into meters instead of pixels
146
147 %% Calculate flame speeds from H
148
149 s            = (H.^2 + r^2).^(0.5);
150 ConeArea     = pi*r*s;
151 ST           = v_dot./ConeArea;
152
153 %% Plot
154
155 %% Plot
156
157 lwidth   = 1.5;
158 fsize    = 14;
159 figure;
160 set(gcf, 'color', 'w');
161 subplot(1,4,1); imagesc(Intensity(:, :)); axis image; title('
      Cropped');
162 subplot(1,4,2); imagesc(Axisym(:, :)); axis image; title('
      Axisymmetric');
163 subplot(1,4,3); imagesc(ImageFilt(:, :)); axis image; title('
      Filtered');
164 subplot(1,4,4); imagesc(ImageAbel(:, :)); axis image; title('
      Abel Transformed');
165
166 figure;
167 set(gcf, 'color', 'w');
168 plot(100*met, CL, 'r', 100*met, GF, 'b', 'LineWidth', lwidth);
169 set(gca, 'FontSize', fsize, 'FontName', 'Times');
170 xlabel('axial location (cm)');
171 ylabel('Intensity');
```

```
172
173 figure;
174 set(gcf, 'color', 'w');
175 subplot(111); imagesc(ImageFilt(:, :)); axis image; title('
    Axisym');
176
177 figure;
178 set(gcf, 'color', 'w');
179 subplot(111); imagesc(ImageAbel(:, :)); axis image; title('Abel
     Transformed');
180
181 figure;
182 set(gcf, 'color', 'w');
183 plot(100*met, CL ./ max( CL), 'r', 'LineWidth', lwidth); hold
    on
184 plot(100*met, CL_axisym ./ max(CL_axisym), 'b', 'LineWidth',
    lwidth); hold off
185 xlabel('axial location (cm)');
186 ylabel('Intensity');
187 legend('Abel Transformed Centerline', 'Axisym Image Centerline'
    )
188
189 fprintf('S_T = %5.4f\n',ST)
190
191 save('Calibration_old.mat','Lf','Rf','Bcrop','Right','Left')
```

E.2 Mean Image Calculation (MATLAB)

```
clear
clc
close all

main_filepath = 'D:\High Speed Footage\Raw tiff files';
save_filepath = 'D:\Average Intesities (High Speed)';
fuel_desgination = {'S1'};
pressure_desgination = {'atmospheric'};
s_desgination = {'S1','S2','S3'};
phi_desgination = {'phi 0.85','phi 0.80','phi 0.78','phi 0.76',
    'phi 0.74','phi 0.72','phi 0.70','phi 0.65'};
date = 'Feb\02-09-2019';

tic
for fuel = 1:length(fuel_desgination)
    for pressure = 1:length(pressure_desgination)
        background_filepath = fullfile(main_filepath,
            fuel_desgination{fuel},date,pressure_desgination{
            pressure},'background');
        background_save = fullfile(save_filepath,
            fuel_desgination{fuel},date,pressure_desgination{
            pressure});
        image_averaging(background_filepath,background_save,'
            background');
        for s = 1:length(s_desgination)
            s_filepath = fullfile(main_filepath,
                fuel_desgination{fuel},date,pressure_desgination
                {pressure},s_desgination{s});
            s_save = fullfile(save_filepath,fuel_desgination{
                fuel},date,pressure_desgination{pressure},
```

```
                s_desgination{s});
22              for phi = 1:length(phi_desgination)
23                  phi_filepath =  fullfile(s_filepath,
                        phi_desgination{phi});
24                  image_averaging(phi_filepath,s_save,
                        phi_desgination{phi});
25              end
26          end
27      end
28  end
29  toc
```

```
1   function image_averaging(filepath,savepath,name)
2       % Create a time averaged image from a series of files in
            the
3       % specified directory
4
5       imageData = imageDatastore(filepath); % Load the images
            into an imageDatastore
6
7       runningTotal = double(imageData.readimage(1)); % Initialize
            the running total for the average calcluation
8
9       for image = 2:imageData.numpartitions % Iterate through all
            of the images adding each image element-wise to create
           a running total
10          runningTotal = runningTotal + double(imageData.
                readimage(image));
11      end
12
13      imageAverage = runningTotal ./ imageData.numpartitions; %
            Divide by the total number of images for the average
14
```

```
15      save(fullfile(savepath,strcat(name,'.mat')),'imageAverage')
            ; % Save the cropped image so it can be loaded later
```

E.3 Radial Profile Generation (MATLAB)

```
1  clear
2  clc
3  close all
4
5  %% Fuel file path look up
6  main_filepath = 'C:\Spatial Correlation Code\Average Intesities
       (High Speed)';
7  fuel_path = dir(main_filepath);
8  [FuelTotal, temp] = size(fuel_path);
9
10 for FuelCount = 3:FuelTotal
11 fuel_desgination{FuelCount-2} = fuel_path(FuelCount).name;
12 end
13
14 s_desgination = {'S1','S2','S3'};
15
16 for fuel = 1:length(fuel_desgination)
17     %% Date file path look up
18     date_path = dir(fullfile(main_filepath,fuel_desgination{
           fuel}));
19     [DateTotal, temp] = size(date_path);
20
21     for DateCount = 3:DateTotal
22         date_desgination{DateCount-2} = date_path(DateCount).
               name;
23     end
24
25     Index = find(contains(date_desgination,'2019'));
```

```
                                % Runs files only pertaining to
        data collected on certain days
26
27      for date = 1:length(Index)
28
29          %% Crop
30          cal_img = imread(char(fullfile(main_filepath,
                fuel_desgination{fuel},date_desgination(Index(date))
                ,'Calibration.tif')));
31
32          figure
33          imshow(cal_img)
34          colormap('Bone')
35          axis image
36          title('Select Top Edge, Bottom Edge, and Right Edge')
37          [x_flame,y_flame] = ginput(3);
38          top                         = round(y_flame(1));
                                          % left edge of the
                flame
39          bottom                      = round(y_flame(2));
                                          % right edge of the
                flame
40          crop                        = round(x_flame(3));
                                          % location for
                cropping of the top of the image
41
42          Cal = abs(top-bottom)/0.03;
43
44          %% Pressure file path look up
45          pressure_path = dir(char(fullfile(main_filepath,
                fuel_desgination{fuel},date_desgination(Index(date))
                )));
46          [PressureTotal, temp] = size(pressure_path);
```

```
47
48          for PressureCount = 3:PressureTotal
49              pressure_desgination{PressureCount-2} =
                    pressure_path(PressureCount).name;
50          end
51
52          Index_2 = find(contains(pressure_desgination,'atmo'));
                        % Skips the cal image in the folder
53
54          for pressure = 1:length(Index_2)
55              background = load(char(fullfile(main_filepath,
                    fuel_desgination{fuel},date_desgination(Index(
                    date)),pressure_desgination{Index_2(pressure)},'
                    background.mat')));
56              [radius,height] = size(background.imageAverage);
57              for s = 1:length(s_desgination)
58                  s_filepath = fullfile(main_filepath,
                        fuel_desgination{fuel},date_desgination(
                        Index(date)),pressure_desgination{Index_2(
                        pressure)},s_desgination{s});
59                  phi_path = dir(char(strcat(s_filepath,'\*phi*',
                        '.mat')));
60                  [PhiTotal, temp] = size(phi_path);
61                  for PhiCount = 1:PhiTotal
62                      phi_desgination{PhiCount} = phi_path(
                            PhiCount).name;
63                  end
64                  Image_cache_S1 = zeros(radius,height,length(
                        phi_desgination));
65                  Image_cache_S2 = zeros(radius,height,length(
                        phi_desgination));
66                  Image_cache_S3 = zeros(radius,height,length(
                        phi_desgination));
```

```
67              for phi = 1:length(phi_desgination)
68                  if s == 1
69                      Image =  load(char(fullfile(s_filepath,
                            phi_desgination{phi})));
70                      Image_cache_S1(:,:,phi) = Image.
                            imageAverage;
71                  elseif s == 2
72                      Image =  load(char(fullfile(s_filepath,
                            phi_desgination{phi})));
73                      Image_cache_S2(:,:,phi) = Image.
                            imageAverage;
74                  elseif s == 3
75                      Image =  load(char(fullfile(s_filepath,
                            phi_desgination{phi})));
76                      Image_cache_S3(:,:,phi) = Image.
                            imageAverage;
77                  end
78              end
79          end
80          Average_Image = zeros(radius,height,length(
                phi_desgination));
81          for phi = 1:length(phi_desgination)
82          Average = (Image_cache_S1(:,:,phi) + Image_cache_S2
                (:,:,phi) + Image_cache_S3(:,:,phi))./3 -
                background.imageAverage;
83          Average(Average < 0) = 0;
84          Average_Image(:,:,phi) = Average;
85          end
86          colors = {'Black';
87                'Orange';
88                'Sky Blue';
89                'Bluish Green';
90                'Yellow';
```

```
91                      'Blue';
92                      'Vermillion';
93                      'Reddish Purple'};
94                  Radius = [-151:1:152]./Cal*1000;
95                  figure
96                  for phi = 1:length(phi_desgination)
97                      max_intensity(phi) = max(max(Average_Image(:,1:
                            crop,phi)));
98                      [RadialLoc AxialLoc] = find(Average_Image(:,1:
                            crop,phi) == max_intensity(phi));
99                      Radial_Profile = Average_Image(:,AxialLoc,phi)
                            ./max_intensity(phi);
100                     plot(Radius,Radial_Profile,'color',CustomColors
                            (colors{phi}));
101                     hold on
102                 end
103                 title(strcat(fuel_desgination{fuel},
                        pressure_desgination{Index_2(pressure)}))
104                 xl = xlabel('$Radial (mm)$','FontSize',30,'
                        FontWeight','bold');
105                 yl = ylabel('$I/I_{max}$','FontSize',30,'FontWeight
                        ','bold');
106                 set(xl, 'Interpreter', 'latex');
107                 set(yl, 'Interpreter', 'latex');
108                 set(gca,'FontSize',15);
109             end
110     end
111 end
```

E.4 Pocket Determination

```
1 function [number_of_pockets,Total_pocket_area,Total_area] =
      pocket_counting(flame_path,background_path)
```

```
2
3       imageData = imageDatastore(flame_path);
4       background = load(fullfile(background_path,'background.mat'
            ));
5
6   %     image = 13056;
7       for image = 1:imageData.numpartitions
8           flame_sub = imageData.readimage(image) - uint16(
                background.imageAverage);
9           flame_sub(flame_sub < 0) = 0;
10
11
12          se = strel('square',2);
13          flame_binary_raw = imbinarize(flame_sub,graythresh(
                flame_sub));
14          flame_binary_erode = imerode(flame_binary_raw,se);
15          flame_binary = imdilate(flame_binary_erode,se);
16
17  %         figure
18  %         imshow(flame_binary)
19  %         hold on
20
21          [boundary labels number A] = bwboundaries(flame_binary)
                ;
22          index = 1;
23          for k = 1:number
24              if(nnz(A(:,k)) > 0)
25                  b_outeredge = boundary{k};
26  %                 plot(b_outeredge(:,2), b_outeredge(:,1), 'r
    ','LineWidth',2)
27                  for l = find(A(:,k))'
28                      b_pockets = boundary{l};
29  %                   plot(b_pockets(:,2), b_pockets(:,1), 'g
```

```
    ','LineWidth',2)
30                      [x y] = size(b_pockets);
31                      if x >= 10
32                          Pocket_area(index) = polyarea(b_pockets
                                (:,2),b_pockets(:,1));
33                          flame_pockets{index} = boundary{1};
34                          index = index + 1;
35                      end
36                  end
37              end
38          end
39          Total_area(image) = bwarea(flame_binary);
40          if exist('flame_pockets')
41              [bleh number_of_pockets(image)] = size(
                    flame_pockets);
42          else
43              number_of_pockets(image) = 0;
44          end
45          if exist('Pocket_area')
46              Total_pocket_area(image) = sum(Pocket_area);
47          else
48              Total_pocket_area(image) = 0;
49          end
50          clear Pocket_area flame_pockets boundary labels number
                A
51      end
```

E.5 Flow Rate Calculation (EES)

"Flow rate calculations for Jet-A (A2)"

"Refrence States"
T_ref = 273[K]
P_ref = 101.325[kPa]
R = 8.314[kJ/kmol-K]*convert(kJ/kmol-K,kJ/mol-K)

"Molecular Weight"
MW_air =molarmass(Air)*convert(kg/kmol,g/mol)
MW_fuel = 159[g/mol]

"Stoichometric balance of air and fuel mixture, Turns Page 21"
x= 11.4
y = 22.1
a = x + y/4

"Air to Fuel ratio"
AF = 4.76*a/phi*MW_air/MW_fuel

"Total Mass flow rate"
"T_nozzle_exit = 475[K]
P_chamber = 1 [-]"
d = 12[mm]*convert(mm,m)
m_dot_total = pi*viscosity(*Air*,*T*=473[K])*Re*d/4

"Mass Fraction of air"
Y_air = AF/(AF+1)

"Mass Fraction of Fuel"
Y_fuel = 1 - Y_air

"Mass flow rates of fuel and air"
m_dot_air = Y_air*m_dot_total
m_dot_fuel = Y_fuel*m_dot_total

"Volumetric flow rate of fuel and air"
ASTM_Density_A2 = 803[kg/m^3]
Main_Air = m_dot_air*volume(*Air*,*T*=T_ref,*P*=P_ref)*(300/250)*convert(m^3/s,L/min)
Fuel_Pump =m_dot_fuel*(1/ASTM_Density_A2)*convert(m^3/s,mL/min)/2

"Pilot Heat Release Calculations"
LHV_ASTM_A2 = 43.06[MJ/kg]*convert(MJ/kg,kJ/kg)
Q_dot_fuel = m_dot_fuel*LHV_ASTM_A2
Q_dot_CH4 = m_dot_CH4*"50792[kJ/kg]"lowerheatingvalue(CH4)
Q_dot_CH4/Q_dot_fuel = 0.115

"Volmetric Flow rate of CH4"
Pilot_Methane = m_dot_CH4*volume(*CH4*,*T*=T_ref,*P*=P_ref)*convert(m^3/s,L/min)

"Mass flow rate of Pilot Air"
MW_CH4 = molarmass(CH4)*convert(kg/kmol,g/mol)
AF_pilot = 4.76*2*MW_air/MW_CH4
m_dot_pilot_air = AF_pilot*m_dot_CH4

"Volumetric flow rate of Pilot Air"
Pilot_Air = m_dot_pilot_air*volume(*Air*,*T*=T_ref,*P*=P_ref)*convert(m^3/s,L/min)

"MW of entire Mixture"
MW_mix = 1/(Y_air/MW_air + Y_fuel/MW_fuel)

"Percentage of Fuel and Air within Mix"
X_fuel = MW_mix/MW_fuel*Y_fuel
X_air = MW_mix/MW_air*Y_air

"Density of the fuel at nozzle exit temperature"
rho_fuel = P_ref*P_chamber*MW_fuel/(R*T_nozzle_exit)

"Unburned density"
rho_u = X_fuel*rho_fuel***convert**(g/m^3,kg/m^3) + X_air***density**(***Air***, ***T***=T_nozzle_exit, ***P***=P_ref*P_chamber)

Parametric Table: Table 1

	Re	$\dot{m}_{total}$	ϕ	$P_{chamber}$ [-]	$T_{nozzle,exit}$ [K]	$Main_{Air}$	$Pilot_{Air}$	$Pilot_{Methane}$	$Fuel_{Pump}$
Run 1	12000	*0.002914*	1	1	473	*151.9*	*14.68*	*1.542*	*6.94467*
Run 2	5000	*0.001214*	0.95	1	473	*63.5*	*5.828*	*0.6122*	*2.75773*
Run 3	5000	*0.001214*	0.9	1	473	*63.7*	*5.539*	*0.5818*	*2.62097*
Run 4	5000	*0.001214*	0.85	1	473	*63.91*	*5.248*	*0.5513*	*2.48333*
Run 5	5000	*0.001214*	0.8	1	473	*64.12*	*4.955*	*0.5205*	*2.34480*
Run 6	5000	*0.001214*	0.75	1	473	*64.32*	*4.661*	*0.4896*	*2.20538*
Run 7	5000	*0.001214*	0.7	1	473	*64.53*	*4.364*	*0.4584*	*2.06505*
Run 8	5000	*0.001214*	0.65	1	473	*64.74*	*4.066*	*0.4271*	*1.92380*
Run 9	5000	*0.001214*	0.6	1	473	*64.95*	*3.765*	*0.3955*	*1.78163*

Parametric Table: Table 1

	ρ_u
Run 1	*0.7874*
Run 2	*0.7853*
Run 3	*0.7833*
Run 4	*0.7813*
Run 5	*0.7792*
Run 6	*0.7772*
Run 7	*0.7751*
Run 8	*0.7731*
Run 9	*0.771*

Appendix F: Burner Operational Procedure

Turbulent Flame Burner Start-up and Shut-down Procedures

Enter the date and then initial the box for each step after it has been completed.

	Date:					

Start up Procedure - Area Set-up

Area and lab set up is critical to safe operation of the device. This check list must be performed prior to burner start up.

1	Clean up area immediately around burner and remove any potentially flammable items					
2	Inform all personnel in lab of pending test and verify they have sufficient PPE					
3	Turn on Power Supply for the MFC units					
4	Let controllers warm-up with no flow for >30 mins					
5	After warm-up, press and hold the zero flow condition button located on the controllers for 3 seconds					

Start-up Pressure System Start-up

This procedure must be followed explicitly for safe operation of the turbulent flame burner. Do not skip or substitute any steps. Changes must be

Colu	Column2	Column3	Column4	Column5	Column6	Column7
1	Verify all heaters and thermocouples are wired correctly					
2	Turn on pressure transducer power supply					
3	Plug in 120 VAC (Black power cord) for heater control board					
4	Verify that 240V safety switch is in the off postion, plug in 240 VAC					
5	Turn 120V safety switch on					
6	Turn 240V safety switch on					
7	Pull out E-Stop button					
8	Start up LabView vi, TurbulentBurnerInterface.vi.					
9	Turn ¼ turn air supply valve					
10	Using gloves if system is warm, fully open vaporizer inlet needle valve (CCW)					
11	Adjust Premix Air MKS pressure regulator to 70 psig					
12	Adjust Pilot Air MKS pressure regulator to 15 psig					
13	Set Channel 2 Air flow rate to 200 SLM					
14	Verify Flow interlock disengages in VI (Green Light)					
15	Adjust pilot fuel air MKS to desired air flow					
16	Turn 240V safety switch off (red light should turn off)					

17	Push in E-Stop					
18	Using soap spray perform leak check on all air fittings					
19	If leak is found close pressure regulators and main globe valve and repair. If no leaks found proceed					
20	Turn 240V safety switch on					
21	Pull out E-Stop button					
22	Switch silver toggle switches on for all heater control units					
23	Beginning with heater 1 power on all heaters in order by flipping red safety toggles					
24	Open dilutant valve (if applicable)					
25	**Allow system to steady state**					
26	Plug power and data wires in UV camera					
27	Turn camera on (feel air blowing above fan)					
28	Take out lens cover					
29	Open Andor Solis software					
30	Cool down camera to -15^{o}C					
31	Make folder with today's date in appropriate folder for both computers					
32	When camera is cooled down -> load config files: turbulent flame settings, then press F3					
33	In Labview, populate filename with today's folder and test number					
34	Retrieve general fuel catch container from flammable liquid storage and connect to fuel return line on lab bench					
35	Insert fuel draw line into desired fuel container					
36	Power on Isco pump controller and pumps					
37	Open Gas Cage and open Methane and Nitrogen Tanks					
38	On Gas panels, open the CH4 and N2 lines by turning the quarter turn valves					

Shut-down Procedure - System Shut-down

Safe system shutdown is critical to prevent potential damage to the system and avoiding any potential accidents. Follow the listed procedure exactly.

1	Engage Nitrogen Purge (nitrogen purge will stop when button is released)					
3	Increase Air flow rate to maximum					
	In the Gas Cage, close off Methane and Nitrogen tanks. Lock up cage.					

	On gas panels, turn of CH4 and N2 lines by turning the qauter turn valves					
4	Shut down all heaters one by one					
5	Once all heaters have been shut off, turn off 240V switch (red light should turn off)					
6	Depress E-Stop button					
	Unplug 240 VAC line					
8	Turn off methane flow on MKS controller screen					
9	Allow system to flow with all heaters disengaged until burner thermocouple registers at 40 °C or below					
10	Once system has cooled fully close air flow pressure regulators					
11	Close ¼ turn main air supply valve					
12	Move all heater controller unit switches to off position					
13	Turn heater controller safety key switch 1 to off position					
14	Unplug 120 VAC line					
15	Turn off power supply for the MKS units using the LED screen (esc from flow screen, then press 0)					
16	Stop Lab VIEW VI and close program (hit the Stop button, on the VI, not the stop button in LabView next to the run button).					
17	Remove fuel draw line from fuel container, and put container in flammables storage					
18	Empty Fuel redirect tank into secondary fuel storage container if more than 1 gallon of fuel is present					

Bibliography

[1] *Standard Inputs for EUROCONTROL Cost Benefit Analyses*, 7th ed. Eurocontrol, 2015.

[2] (2016). Fast facts on transportation greenhouse gas emissions, [Online]. Available: https://www.epa.gov/greenvehicles/fast-facts-transportation-greenhouse-gas-emissions.

[3] A. S. Gohardani, G. Doulgeris, and R. Singh, "Challenges of future aircraft propulsion: A review of distributed propulsion technology and its potential application for the all electric commercial aircraft", *Progress in Aerospace Sciences*, vol. 47, pp. 369–391, 2011. DOI: 10.1016/j.paerosci.2010.09.001.

[4] A. H. Epstein, "Aircraft engines' needs from combustion science and engineering", *Combustion and Flame*, vol. 159, pp. 1791–1792, 2012. DOI: 10.1016/j.combustflame.2012.02.022.

[5] "European aviation safety agency certification specification, cs-e 910", 2003.

[6] "Federal aviation regulation, section 25.903", 2000.

[7] T. Lieuwen, V. McDonell, E. Petersen, and D. Santavicca, "Fuel flexibility influences on premixed combustor blowout, flashback, autoignition, and stability", *Combustion and Fuels, Education*, vol. 1, pp. 601–615, 2008.

[8] X. Hui and S. C. J, "Laminar flame speeds of transportation-relevant hydrocarbons and jet fuels at elevated temperatures and pressures", *Fuel*, vol. 109, pp. 191, 200, 2013. DOI: 10.1016/j.fuel.2012.12.084.

[9] K. Kumar, C. Sung, and X. Hui, "Laminar flame speeds and extinction limits of conventional and alternative jet fuels", *Fuel*, vol. 90, pp. 1004, 1011, 2011. DOI: 10.1016/j.fuel.2010.11.022.

[10] D. Dunn-Rankin, *Lean Combustion*. Academic Press, 2008, ISBN: 9780123706195.

[11] S. Bray, *Turbulent Premixed Flames*. Cambridge University Press, 2011, ISBN: 9780521769617.

[12] F. Carbone, J. L. Smolke, A. M. Fincham, and F. N. Egolfopoulos, "Comparative behavior of piloted turbulent premixed jet flames of c1-c8 hydrocarbons", *Combustion and Flame*, vol. 180, pp. 88–101, 2017.

[13] J. A. Fillo, "The global consumption speeds of premixed large-hydrocarbon fuel/air turbulent bunsen flames", PhD thesis, Oregon State University, 2016.

[14] S. Dooley, S. H. Won, M. Chaos, J. Heyne, Y. Ju, F. L. Dryer, K. Kumar, C. J. Sung, H. Wang, M. A. Oehlshlaeger, R. J. Santoro, and T. A. Litzinger, "A jet fuel surrogate formulated by real fuel properties", *Combustion and Flame*, vol. 157, pp. 2333, 2339, 2010. DOI: 10.1016/j.combustflame.2010.07.001.

[15] K. Kumar, J. E. Freeh, C. J. Sung, and Y. Huang, "Laminar flame speeds of preheated iso-octane/o2/n2 and n-heptane/o2/n2 mixtures", *Journal of Propulsion and Power*, vol. 23, no. 2, pp. 428, 436, 2007. DOI: 10.2514/1.24391.

[16] C. K. Law, *Combustion Physics 1st ed.* Cambridge University Press, 2006, ISBN: 9780521870528.

[17] "An introduction to combustion: Concepts and applications", in, S. R. Turns, Ed. New York: McGraw-Hill Education, 2011, p. 457.

[18] P. Venkateswaran, A. Marshall, S. J. M, and L. T. C, "Turbulent consumption speeds of high hydrogen content fuels from 1-20 atm", *Journal of Engineering for Gas Turbines and Power*, vol. 136, pp. 1, 8, 2014. DOI: 10.1115/1.4025210.

[19] H. Kobayash, "Experimental study of high-pressure turbulent premixed flames", *Experimental Thermal and Fluid Science*, vol. 26, pp. 375, 387, 2002. DOI: 10.1016/S0894-1777(02)00149-8.

[20] A. L. ans J. Chomiak, "Turbulent flame speed and thickness: Phenomenology, evaluation, and application in multi-dimensional simulations", *Progress in Energt and Combustion Science*, vol. 28, pp. 1–74, 2002.

[21] R. Fragner, F. Halter, N. Mazellier, C. Chauveau, and I. Gökalp, "Investigation of pressure effects on the small scale wrinkling of turbulent premixed bunsen flames", *Proceedings of the Combustion Institute*, vol. 35, pp. 1527–1535, 2015.

[22] B. Coriton, J. H. Frank, and A. Gomez, "Interaction of turbulent premixed flames with combustion products: Role of stoichiometry", *Combustion and Flame*, vol. 170, pp. 37–52, 2016.

[23] T. Edwards, "Reference jet fuels for combustion testing", *55th AIAA Aerospace Sciences Meeting*, AIAA 2017-0146. DOI: 10.2514/6.2017-0146.

[24] E. T. Turgut, T. H. Karakoc, and A. Hepbasli, "Exergetic analysis of an aircraft turbofan engine", *International Journal of Energy Research*, vol. 31, pp. 1383, 1397, 2007. DOI: 10.1002/er.1310.

[25] Y. Wu, V. Modica, B. Rossow, and F. Grisch, "Effects of pressure and preheating temperature on the laminar flame speed of methane/air and acetone/air mixtures", *Fuel*, vol. 185, pp. 577, 588, 2016. DOI: 10.1016/j.fuel.2016.07.110.

[26] F. N. Egolfopoulos, P. Cho, and C. K. Law, "Laminar flame speeds of methane-air mixtures under reduced and elevated pressures", *Combustion and Flame*, vol. 76, pp. 375, 391, 1989. DOI: 10.1016/0010-2180(89)90119-3.

[27] T. Ombrello, C. Carter, and V. Katta, "Burner platform for sub-atmospheric pressure flame studies", *Combustion and Flame*, vol. 159, pp. 2363, 2373, 2016. DOI: 10.1016/j.combustflame.2012.03.010.

[28] W. Lowry, J. Vries, M. Krejci, E. Petersen, Z. Serinyel, W. Metcalfe, H. Curran, and G. Bourque, "Lamianr flame speed measurements and modeling of pure alkanes and alkane blends at elevated pressures", *Journal of Engineering for Gas Turbines and Power*, vol. 133, pp. 1–9, 2011. DOI: 10.1115/1.4002809.

[29] M. Kuznetsov, S. Kobelt, J. Grune, and T. Jordan, "Flammability limits and laminar flame speed of hydrogen-air mixtures at sub-atmospheric pressures", *International Journal of Hydrogen Energy*, vol. 37, pp. 17 580–17 588, 2012. DOI: 10.1016/j.ijhydene.2012.05.049.

[30] A. D. Marshal, P. Venkateswaran, J. M. Seitzman, and T. C. Lieuwen, "Pressure effects on the turbulent consumption speeds of high h2 mixtures", in *Power for Land, Sea and Air*, ser. GT2012-68305, Copenhagen, Denmark: ASME, 2012, pp. 1–11.

[31] H. Kobayash, K. Y, and M. K, "Experimental study on general correlation of turbulent burning velocity at high pressure", *Symposium (International) on Combustion*, vol. 27, pp. 941, 948, 1998. DOI: 10.1016/s0082-0784(98)80492-X.

[32] L. J. Jiang, S. S. Shy, W. Y. Li, H. M. Huang, and M. T. Nguyen, "High-temperature, high-pressure burning velocities of expanding turbulent premixed flames and their comparison with bunsen-type flames", *Combustion and Flame*, vol. 172, pp. 173, 182, 2016. DOI: 10.1016/j.combustflame.2016.07.021.

[33] P. Venkateswaran, A. Marshall, D. H. Shin, and D. Noble, "Measurements and analysis of turbulent consumption speeds of h2/co mixtures", *Combustion and Flame*, vol. 158, pp. 1602, 1614, 2011. DOI: 10.1016/j.combustflame.2010.12.030.

[34] C. K. Law and C. J. Sung, "Structure, aerodynamics, and geometry of premixed flamelets", *Progress in Energy and Combustion Science*, vol. 26, pp. 459–505, 2000.

[35] V. Akkerman and V. Bychkov, "Turbulent flame and the darrieus-landau instability in a three-dimensional flow", *Combustion Theory and Modelling*, vol. 7, pp. 767–794, 2003.

[36] J. Yuan, Y. Ju, and C. K. Law, "Effects of turbulence and flame instability on flame front evolution", *Physics of Fluids*, vol. 18, 2006.

[37] J. Wang, Y. Nie, X. Cai, S. Guo, W. Zhang, and Y. Xie, "Investigation on the highly negative curved syngas bunsen flame and the critical local karlovitz number when tip opening", *Fuel*, vol. 215, pp. 429–437, 2018.

[38] C. K. Law, S. Ishizuka, and P. Cho, "On the opening of premixed bunsen flame tips", *Combustion Scince and Technology*, vol. 28, pp. 89–96, 1982.

[39] A. J. Fillo, J. M. Bonebrake, and D. Blunck, "Impact of fuel chemistry and stretch rate on global consumption speed of large hydrocarbon fuel/air flames", *National Combustion Meeting*, vol. 31, pp. 1, 12, 2017.

[40] D. Guyot, F. Guethe, B. Schuermans, A. Lacarelle, and C. O. Pascheret, "Ch*/oh* chemiluminescence response of an atmospheric premixed flame under varying operating conditions", in *Power for Land, Sea and Air*, ser. GT2010-23135, Glasgow, UK: ASME, 2012, pp. 1–12.

[41] C. J. Dash, "One-dimensional tomography: A comparison of abel, onion-peeling and filtered backprojection", *Applied Optics*, vol. 31, pp. 1146, 1152, 1992. DOI: 10.1364/AO.31.001146.

[42] R. Xu, K. Wang, S. Banerjee, J. Shao, T. Parise, Y. Zhu, S. Wang, A. Movaghar, D. J. Lee, R. Zhao, X. Han, Y. Gao, T. Lu, K. Brezinsky, F. N. Egolfopoulos, D. F. Davidson, R. K. Hanson, C. T. Bowman, and H. Wang, "A physics-based approach to modeling real-fuel combustion chemistry - ii. reaction kinetic models of jet and rocket fuels", *Combustion and Flame*, vol. 193, pp. 520, 537, 2018. DOI: 10.1016/j.combustflame.2018.03.021.

[43] C. Ji, S. M. Sarathy, P. S. Veloo, C. K. Westbrook, and F. N. Egolfopoulos, "Effects of fuel branching on the propagation of octane isomers flames", *Combustion and Flame*, vol. 159, pp. 1426–1436, 2011. DOI: 10.1016/j.combustflame.2011.12.004.

[44] S. M. Sarathy, U. Niemann, C. Yeung, R. Gehmlich, C. K. Westbrook, M. Polmer, Z. Luo, M. Mehl, W. J. Pitz, K. Seshadri, M. J. Thomson, and T. Lu, "A counterflow diffusion flame study of branched octane isomers", *Proceedings of the Combustion Institute*, vol. 34, pp. 1015–1023, 2012. DOI: 10.1016/j.proci.2012.05.106.

[45] D. Veynante and T. Poinsot, "Effects of pressure gradients on turbulent premixed flames", *Journal of Fluid Mechanics*, vol. 353, pp. 83–114, 1997.

[46] K. Kumar and C. J. Sung, "A comparative experimental study of the autoignition characteristics of alternative and conventional jet fuel/oxidizer mixtures", *Fuel*, vol. 89, pp. 2853–2863, 2010. DOI: 10.1016/j.fuel.2010.02.021.

[47] M. Colket, T. Edwards, S. Williams, N. P. Cernansky, D. L. Miller, F. Egolfopoulos, P. Lindstedt, K. Seshadri, F. L. Dryer, C. K. Law, D. Friend, D. B. Lenhert, H. Pitsch, A. Sarofim, M. Smooke, and W. Tsang, "Development of an experimental database and kinetic models for surrogate jet fuels", *45th AIAA Aerospace Sciences Meeting and Exhibit*, vol. 724, pp. 1–21, 2007.

[48] J. F. Driscoll, "Turbulent premixed combustion: Flamelet structure and its effect on turbulent burning velocities", *Progess in Energy and Combustion Science*, vol. 34, pp. 91–134, 2008. DOI: 10.1016/j.pecs.2007.04.002.

[49] N. E. Schorn, J. Bonebrake, and D. L. Blunck, "Flame stability of turbulent premixed jet flames of large hydrocarbon fuels", *Western States Section of the Combustion Institute*, pp. 1, 7, 2017.

[50] H. Brunn, *Hot wire anemometry: principles and signal analysis*. Oxford University Press, 1995, ISBN: 9781420085341.

[51] E. P. H. S. Linow, "Laser diagnostics for studies of turbulent combustion", *Measurement Science and Technology*, vol. 11, pp. 37–57, 2000. DOI: 10.1088/0957-0233/11/2/201.

[52] N. Otsu, "A threshold selection method from gray-level histograms", *IEEE*, vol. 9, pp. 62–66, 1978.

[53] R. Gonzalez, R. Woods, and S. Eddins, *Digital Image Processing Using MATLAB*. Gatesmark Publishing, 2009, ISBN: 978-0982085400.

[54] R. Gonzalez, R. Woods, and S. Eddins, *Digital Image Processing Using MATLAB*. Prentice Hall PTR, 2004, ISBN: 978-01300851910.

[55] R. va den Boomgard and R. van Balen, "Methods for fast morphological image transforms using bitmapped images", *Computer Vision, Graphics, and Image Processing: Graphical Models and Image Processing*, vol. 54, pp. 252–254, 1992.